

https://dspace.org/

A documentation of the morphology of the lungs of the Sprague Dawley rat after chronic heat exposure

Peya, Yolanda

2023

University of the Witwatersrand, Johannesburg

https://hdl.handle.net/10539/43212

Peya, Yolanda. (2023). A documentation of the morphology of the lungs of the Sprague Dawley rat after chronic heat exposure [Master's dissertation, University of the Witwatersrand, Johannesburg]. WireDSpace.

Downloaded from a DSpace repository. https://dspace.org/

A DOCUMENTATION OF THE MORPHOLOGY OF THE LUNGS OF THE SPRAGUE DAWLEY RAT AFTER CHRONIC HEAT EXPOSURE

Yolanda Peya

(1123409)



A dissertation submitted to the Faculty of Health Sciences, University of the Witwatersrand, Johannesburg, in fulfilment of the requirements for the degree of Master of Science in Medicine

Johannesburg, 2023

Declaration

I, Yolanda Peya, declare that this Dissertation is my own, unaided work. It is being submitted for the Degree of Master of Science in Medicine(Anatomical Sciences) at the University of the Witwatersrand, Johannesburg. It has not been submitted before for any degree or examination at any other University.

Yolanda Peya

(Signature of Candidate)

Signed at the University of the Witwatersrand, Johannesburg, South Africa on the 11th day of December 2023.

Dedication

In memory of my grandmother - Celiwe Mavis Ditala

This dissertation is dedicated to my parents – Dr Bukiwe Peya and Mr Luyanda Skosana.

Thank you for the guidance, unwavering support and for all your sacrifices.

Abstract

Climate change is a natural phenomenon that is exacerbated by multiple human activities in the environment. These activities lead to a rise in global temperatures. This increases the occurrence of heatwaves which pose a major threat to ecosystems, biodiversity, and the conservation of species on Earth. This study, aimed to document the effects of chronic heat exposure on the lungs of the Sprague Dawley rat using histological and immunofluorescence techniques. Twenty-four (24) rats were assigned to three groups; each exposed to different temperatures; (i) group A (n = 8) exposed to 25 °C (ii) group B (n = 8) exposed to 33 °C and (iii) group C (n = 8) exposed to 34 °C. This was done for a period of 4 weeks and the rats were euthanised thereafter. Methods employed included Intratracheal instillation, and histological and immunofluorescence techniques. This study found that rats in group A (25 °C) displayed no structural adaptations in comparison to groups B and C. Enlarged blood vessels with thick smooth muscle and prominent elastic fibres, bronchus-associated lymphoid tissue (BALT), and increased collagen deposition were observed in group B (33 °C). These indicate the activation of immune responses and adaptation to new environmental temperatures. In group C (34 °C), the lung morphology was severely damaged. There was an increased loss of epithelial integrity, oedema, pulmonary alveolar proteinosis (PAP), and a severe decrease in the lung-to-surface area ratio. The significant changes caused by the 1 °C temperature difference between groups B (33 °C) and C (34 °C) illustrate the detrimental effects of chronic heat stress. It is evident that increasing environmental temperatures due to climate change is harmful to life and immediate interventions are necessary to combat rising temperatures.

Acknowledgements

I would like to extend my unreserved gratitude to my supervisor, Dr. Deran Reddy for his eagerness to always teach and share knowledge, unwavering support, time and guidance throughout my Master's Degree.

I wish to thank Dr. Abdurrahman Abdulkadir for his guidance and advice throughout this journey. I would also like to thank Dr. Nura Bello Kaura for assisting me in the lab, even during the weekends. Thank you for also proofreading my work, your assistance has made an immense difference. You have played a pivotal role in ensuring that I finish strong. A special thank you to Mrs Ali for cheering me up when my immunofluorescence experiment failed the first time. Thank you for assisting and ensuring I finally get it right.

I would like to thank my parents, Dr B. Peya and Mr L. Skosana, for their financial and emotional support. I'll forever be indebted to you guys. To my grandmother, Nomntu Jantjies Peya, your prayers have carried me through. To my dearest friend, Sinoxolo Qeqe, thank you so much for assisting me in every way possible to ensure that I submit on time. I would like to thank my best friends, Okuhle and KB for always supporting, and cheering me on.

To my lovely siblings, Musa, Cebo and Xoli, thank you for being patient with me and understanding my busy schedule. Now that I'm done with this dissertation, we will have countless ice cream and movie dates.

The NRF is highly acknowledged for their funding of this project. The School of Anatomical Sciences and MMU is acknowledged.

Table of contents

Declaration II

Dedication III

Abstract IV

Acknowledgements V

List of Figures X

List of tables XIII

List of abbreviations XIV

1. Introduction 1

1.1. Literature Review 1

1.1.1. The rise of climate change 1

1.1.2. The Impact of Climate Change on Biodiversity and Life on Earth 2

1.1.3. The Rise in Global Temperatures 3

1.1.4. Synopsis of Heatwaves 4

Effects of heatwaves on humans 4

Effects of heatwaves on plants and animals 5

1.1.5. Heat Acclimation and Heat-related Illnesses in Endothermic Species 6

Endotherms and the mechanism of thermoregulation 6

1.1.6. Heat Stress 7

1.1.7. Heat Acclimation 8

Phases of heat acclimation 9

1.1.8. Structure and Function of the Respiratory System of the Sprague Dawley Rat 10

The Origins of the Sprague Dawley Rat 10

Sprague Dawley Rats as Models of Scientific Research 11

The Respiratory System of the Sprague Dawley Rat 11

Structure of the Pulmonary Blood-Gas Barrier 13

1.2. Rationale for the Study 15

1.3. Aim and Objectives 17

2. Material and Methods 18

2.1. Study animals 18

2.2. Experimental Design 18

Chamber description 19

2.3. Intra-tracheal Instillation 22

2.4. Latex Casting 23

2.5. Gross Morphology 25

2.6. Histology 25

Sampling of Lung Tissue 25

2.7. Light Microscopy 27

Tissue Processing, Embedding and Sectioning of the Sampled Lung Tissue 27

Mayer's H&E Stain 28

Modified Verhoeff Elastic Van Gieson's stain 28

Periodic Acid- Schiff Stain 28

New Pentachrome stain 29

RGB Trichrome stain 29

2.8. Immunofluorescence labelling procedures 30

Antibodies Optimisation 30

Immunofluorescence triple labelling 31

2.9. Microscopy 32

2.10. Morphometry 32

2.11. Statistical analysis 33

3. Results 34

3.1. Gross Morphology 34

3.2. Light Microscopy Analyses 35

3.3. Histomorphometry 49

3.4. Immunofluorescence Microscopy Analyses 52

4. Discussion 62

5. Conclusion 69

5.1. Recommendations 69

5.2. Study Limitations 70

6. Reference List 71

7. Appendices 84

Appendix 1: Turnitin Report 84

Appendix 2: Ethics waiver 85

Appendix 3: Ethics approval certificate 86

Appendix 4: Tissue Processing 87

Appendix 5: Haematoxylin and Eosin staining 88

Appendix 6: New pentachrome stain 89

Appendix 7: Van Geison Stain 90

Appendix 8: Red Green Blue (RGB) Trichrome Stain 91

Appendix 9: Periodic Acid- Schiff (PAS) 92

Appendix 10: Immunofluorescence Triple Labelling 93

List of Figures

Figure 1: A diagram of the blood-gas barrier. ……14

Figure 2: The diagram depicts a heat chamber that housed Sprague Dawley Rats in eight cages…….20

Figure 3: An overview of the experimental design highlighting the workflow……21

Figure 4: A Ventral view of the rat's gross morphology……22

Figure 5: The equipment used for latex casting……24

Figure 6: A diagram depicting the systematic regional sampling procedure for obtaining lung samples……26

Figure 7: Images of the gross Morphology of the lungs from control and treatment groups……34

Figure 8: Micrographs of the new pentachrome and RGB stained sections……36

Figure 9: Micrographs of Mayers H&E and new pentachrome stained sections of the lung parenchyma from the control and treatment groups……38

Figure 10: Micrographs of RGB trichrome stained sections of the lung displaying bronchioles from the control and treatment groups……40

Figure 11: Micrographs of new pentachrome and Mayer's H&E-stained sections of the bronchiole from the control and treatment groups……41

Figure 12: Micrographs of Mayer's H&E and PAS-stained sections displaying the alveoli architecture from the control and treatment groups……43

Figure 13: Micrographs of RGB trichrome stained sections displaying collagen deposition around the alveoli from control and treatment groups……..44

Figure 14: Micrographs of Mayer's H&E-stained section displaying enlarged alveolar space from treatment group C (34 °C)……..45

Figure 15: Micrographs of Modified Verfhoeff van Gieson stained sections of the blood vessels from the control and treatment groups ……47

Figure 16: A graph displaying the mean Alveolar size of each group……49

Figure 17: A graph displaying the mean thickness of the interalveolar septa……50

Figure 18: Micrographs of the immunolabelled sections of the lung parenchyma of the control and treatment groups. ……..53

Figure 19: Micrographs of the immunolabelled sections displaying the bronchiole of group A (25 °C)……55

Figure 20: Micrographs of the immunolabelled sections displaying the bronchiole of group B (33 °C)……56

Figure 21: Micrographs of the immunolabelled sections displaying the bronchiole of treatment group C (34 °C)……..57

Figure 22: Micrographs of immunolabelled sections displaying the blood vessel of group A (25 °C)……59

Figure 23: Micrographs of the immunolabelled sections displaying blood vessels of group B (33 °C)……60

Figure 24: Micrographs of the immunolabelled sections displaying blood vessels of group C (34 °C)……61

List of tables

Table 1: Summary of the lung structural alterations and observation after chronic heat exposure……48

Table 2: The morphometric values of alveolar size and septal thickness in the three groups……51

List of abbreviations

A = Alveolus

AD =Alveolar duct

ARDS = Acute respiratory distress syndrome

AREC = Animal Research Ethics Committee

AS = Alveolar sac

B = Bronchiole

BALT = Bronchiole Associated Lymphoid Tissue

BGB = Blood Gas Barrier

BV = Blood vessels

C = Collagen

Ca = Caudal

CC = Clara Cells

CO_2 = Carbon Dioxide

Anti-COL2 = Anti-Collagen II

COPD = Chronic Obstructive Pulmonary Disease

Cr = Cranial

CT = Connective Tissue

DAPI = 6-Diamidino-2-Phenylindole, Dihydrochloride

E = Epithelium

Er= Erythrocytes

EAS = Enlarged alveolar space

ECM = Extracellular Matrix

EF = Elastic Fibres

GHG = Greenhouse Gas

H&E = Haematoxylin and Eosin

HA = Heat Acclimation

HSP = Heat Shock Proteins

HSR = Heat Shock Response

IAS = Interalveolar Septa

IC = Immune Cells

IPCC = Intergovernmental Panel On Climate Change

LTHA = Long Term Heat Acclimation

LYM = Lymphocytes

M = Macrophages

M = Middle

N = Neutrophils

O = Oedema

PAP = Pulmonary Alveolar Proteinosis

PAS = The Periodic Acid Schiff

PFC = Perivascular Fluid Cuffs

RB = Respiratory Bronchiole

RGB = Red-Green-Blue

ROS = Reactive Oxygen Species

S = Surfactant

SA: V = Surface Area to Volume Ratio

SD = Sprague Dawley

Sprague Dawley rats = *Rattus norvegicus domesticus*

STHA = Short Term Heat Acclimation

Heat Acclimation

TB = Terminal Bronchiole

TNZ = Thermoneutral Zone

Type I = Type I Pneumocytes

Type II = Type II Pneumocytes

WRAF = Wits Research Animal Facility

anti-α-SMA = Anti-Alpha-Smooth Muscle Actin

1. Introduction

1.1. Literature Review

1.1.1. The rise of climate change

Climate change is a gradual and persistent change in temperatures and weather patterns that are naturally occurring on a global scale (Chakraborty *et al*., 2014; Santos & Bakhshoodeh, 2021; Abbass *et al*., 2022). Over the years, human activities such as air and water pollution, urbanisation, and industrialisation have remained the leading cause of climate change (Li *et al.,* 2022; Ahmed *et al*., 2022; IPCC, 2022; Mentel *et al*., 2022). These activities greatly burden energy resources and produce extreme levels of carbon dioxide (CO_2) in the atmosphere (Abbass *et al*., 2022; Mentel *et al*., 2022).

The emission of CO_2 is a natural phenomenon that results from natural and man-made processes such as respiration decomposition and combustion (Ahmed *et al*., 2022). The production of high levels of CO_2 in the atmosphere has led to a radical increase in the levels of greenhouse gas (GHG) emissions in the past century (Ahmed *et al.,* 2022; Simandan, 2009). High CO_2 concentrations disrupt natural weather patterns, increase droughts, wildfires, heavy precipitation and elevate global temperatures and sea levels (Ahmed *et al*., 2022; Abbass et al., 2022; IPCC, 2022; USEPA, 2023). Consequently, global ecosystems, biodiversity, and the conservation of human and animal species face severe threats due to constant habitat transformations (Ahmed *et al*., 2022; Abbass *et al*., 2022; USEPA, 2023; IPCC, 2022).

1.1.2. The Impact of Climate Change on Biodiversity and Life on Earth

The impact of industrialisation on the environment varies across different regions of the world (Ahmed *et al*., 2022). The common impact observed in most environments includes air and water pollution, drought, as well as the loss of ecosystems and biodiversity due to deforestation (Ahmed *et al*., 2022; IPCC, 2022). Animal species are therefore at risk of exposure to extreme weather conditions. Only those with a high rate of adaptability will be able to thrive in this challenging environment (Abbass *et al.,* 2022). As such, many studies reported that climate change has caused the extinction of numerous species, and many more are at risk (Abbass *et al.,* 2022). To put this into context, South Africa is the sixth out of the 17 mega biodiversity countries in the world. However; despite its abundant wildlife, alarming statistics show that 14% of plants, 17% of mammals, and 15% of birds are currently at risk of extinction(Scholes & Engelbrecht, 2021).

Mentel *et al*., (2022) found a positive correlation between industrialisation and the production of high carbon dioxide emissions in Sub-Saharan Africa. According to the Intergovernmental Panel on Climate Change (IPCC, 2022), an average of 3.3 to 3.6 billion people live in developing regions of Africa, South Asia, and Central and South America. The increasing rate of urbanisation can be attributed to the rise in global temperatures (Li *et al.,* 2022). Moreover; the United Nations (2019) proposed that urbanisation will occur at a larger scale than before in African countries. More specifically, it is proposed that by 2040, the urban African population will double to more than 1 billion (Toesland, 2019). Since African countries are still developing, they consist of a high density of informal areas (Hugo, 2023). Interestingly, these areas are more vulnerable to climate change due to inequality, poverty, and lack of

resources to cope with extreme conditions. (Hugo, 2023; IPCC, 2022). Additionally, strategies required for adapting to climate change are rarely implemented in informal contexts (Hugo, 2023). As such, the number of deaths due to extreme weather conditions such as droughts and floods in these regions were significantly higher than in developed countries between the years 2010 and 2020 (IPCC, 2022).

1.1.3. The Rise in Global Temperatures

According to Ahmed *et al*., (2022), global temperatures have increased by 06 °C from normal ranges. Additionally, the decade from 2011 to 2020 was the warmest on record, with an average global temperature of 1.1°C (National Centres for Environmental Information, 2021). A recent report formulated by the IPCC projected that by 2031, global temperature ranges will increase by 1.5 to 2 °C (IPCC, 2021; Li *et al.,* 2022).

Similarly, statistics revealed that African countries experienced an increase in average yearly temperatures between 1994 and 2005, which averaged 1.5 °C, 2 °C, and 3 °C. This was reported to be warmer than they were between 1995 to 2014 (0.6 °C, 1.1 °C, and 2.1 °C) (Li *et al.,* 2022). The temperature increases in some countries in Africa are higher than the global level of 2 °C (Li *et al.,* 2022).

It is projected that temperatures in Africa will increase considerably, with predictions of 4 to 6 °C across sub-tropical regions and 3 to 5 °C over tropical regions (Engelbrecht *et al.,* 2015; Saylla *et al.,* 2015). It is further reported that sub-tropical regions in Africa experience global temperature increases on a magnified scale of 1.5 to 2 times the global average (Hugo, 2023). Similarly, a study conducted in Cape Town, Republic of South Africa, projected that there will be a substantial temperature increase of 1.9 to 2.3 °C in 2060 (Gintamo *et al.,* 2021).

Correlative to this, it was reported that Cape Town experienced its hottest winter day in 62 years in June 2022 and August 2023, with temperatures averaging 30.9°C and 34°C, respectively (Engel, 2023). Consequently, according to climate change projections, some African regions may experience heatwaves so severe that the sustenance of livelihood will become increasingly difficult unless urgent mitigation measures are taken (Brimicombe *et al.,* 2021).

1.1.4. Synopsis of Heatwaves

Anderson & Bell (2011) state that there are no constant or consistent temperature thresholds, metrics, and periods that make it possible for a universal definition of heatwaves to exist (Ma *et al.,* 2015). They are, however, usually defined as prolonged durations of excessive heat or exposure to warm air that is trapped and constrained in one place due to a high-pressure system in the atmosphere (Anderson & Bell, 2011). Heatwaves are thus characterised by their frequency, intensity, duration, and pose a threat to the well-being of animals and human beings owing to numerous health risks associated with high temperatures (Luber & McGeehin, 2008; Meehl & Tebaldi, 2004).

Effects of heatwaves on humans

Research shows that extreme heat causes more fatalities than any other natural disaster (Petkova *et al.,* 2014; USEPA, 2023; Coates *et al.,* 2014). Examples of this include the heatwave-induced deaths of 700 people in the USA in July 1995 (Greene *et al.,* 2011; Bouchama *et al.,* 2017). Similarly, heatwave-related disasters in Western Europe and Russia resulted in 70 000 and 55 000 deaths in 2003 and 2010, respectively (Hanania *et al.,* 2020; Bouchama *et al*., 2017). The Republic of South Africa also experienced extreme heatwaves

from late 2015 to early 2016. The Northwest province was impacted the worst, with heatwaves that lasted between 12 to 77 days (Kapwata *et al*., 2022). Most importantly, high temperatures and heatwaves introduce several economic and health challenges that affect the well-being and productivity of people (Hugo, 2023).

Although cities aggravate the rise in global temperatures, they are also vulnerable to experiencing extreme heat on an intensified scale (IPCC, 2022; Hugo, 2023). For example, a study by Hugo (2023) based on informal settlements of Johannesburg in the Republic of South Africa, found that people who live in shacks experience severe indoor heat levels that reach up to 35 °C due to the building and roof materials used. People who live in these structures were found to experience heat-related symptoms such as fatigue, discomfort, loss of productivity, and exhaustion in temperature ranges of approximately 26 °C (Hugo, 2023). In temperature ranges between 27 – 31 °C; they experienced muscle cramps, heat exhaustion, and heat stroke (Hugo, 2023). Heart failure, sunburn, skin rashes, and fainting were experienced in temperature ranges that exceeded 41 °C (Hugo, 2023).

Effects of heatwaves on plants and animals

Plants and trees provide shade for wild animals and cools temperature by up to 10 °C (World Economic Forum, 2022). Although they play a role in the dissipation of heat, they can also be affected by extremely high temperatures (World Economic Forum, 2022). Plants and trees need water to grow (Abbass *et al.,* 2022). Climate change, especially extreme heat, reduces water security, which can hinder plant growth and viability (Abbass *et al.,* 2022). Birds located in deserts and other drought-prone places, for example, are at severe risk as they use their wings to cool off, a mechanism that makes them lose water and require more which might not be available (Daly, 2021). As such, animals particularly wildlife, are directly exposed to weather

conditions due to the absence of shelter. Moreover, heatwaves can disrupt the ecosystem in several ways with animals at risk of losing their food, habitats and lives due to the possibility of wildfires (IPCC, 2022; World Economic Forum, 2022). Therefore, urgent mitigation measures need to be taken to ensure the conservation of ecosystems and life on Earth (Brimicombe *et al.,* 2021).

1.1.5. Heat Acclimation and Heat-related Illnesses in Endothermic Species

Endotherms and the mechanism of thermoregulation

Living organisms rely on specific temperature ranges to sustain their lives (Abbass *et al.,* 2022). As such, heatwaves and insufficient acclimatisation induced by high environmental temperatures give rise to heat-related illnesses such as heat stroke and heat stress. This remains a huge concern in public health to date (Lugo-Amador *et al*., 2004; Ebi *et al.,* 2021). Endotherms are species that produce heat from metabolic processes and use it to regulate their body temperature in environments that exceed or fall short of their thermoneutral zone (TNZ) (Boyles *et al*., 2011).

Endotherms face the risk of unsuccessful thermoregulation and a wide range of physiological complications when external environmental temperatures are more than their body temperatures (Boyles *et al*., 2011; Horowitz, 1998; McKechnie & Wolf, 2019). Mammals exhibit a wide range of body temperatures, typically falling within the range of 30 °C to 41 °C (McKechnie & Wolf, 2019). This physiological characteristic has been extensively studied and documented in the academic literature, with numerous theories proposed to explain the adaptive significance of this trait in mammals (McKechnie & Wolf, 2019). Avian species have a TNZ that ranges between 37 °C to 44 °C whilst that of rodents lies between the temperature ranges of 30 °C to 31 °C for mice, and 30 °C to 32 °C for rats (McKechnie & Wolf, 2019;

Hankenson *et al.,* 2018). This is synonymous with the TNZ of lightly clothed humans which ranges from 28 to 29 °C (Ganeshan & Chawla, 2017; Frohlich, 2020).

Endotherms strive to maintain constant body temperatures for optimum activity, health, and lower levels of energy expenditure (Ganeshan & Chawla, 2017). An increase in temperatures beyond the TNZ of species signifies an increase in their metabolic energy as their body works hard to dissipate the accumulated heat (Ganeshan & Chawla, 2017). Endotherms are therefore affected by climate change on multiple functional levels as their ability to acclimate is influenced by the availability of metabolic energy as well as food resources in their external environment (Glanville *et al.,* 2012). Other factors that negatively impact the ability of endotherms to acclimate are intrinsic characteristics (Cole *et al*., 2023). In humans, extreme age individuals are more at risk of age-induced delayed responses which might result in significantly higher body temperatures (Cole *et al*., 2023).

1.1.6. Heat Stress

Heat stress in simplest terms, occurs when individuals or animals are exposed to extreme heat conditions that extend beyond their TNZ (Xiang *et al*., 2014). It is the leading cause of heatstroke, a life-threatening condition that is characterised by hyperthermia and organ failure due to an expeditious increase in body temperature that exceeds 40 °C, resulting in central nervous system dysfunction (Yan *et al.,* 2006; Bouchama *et al.,* 2017; Bouchama *et al*., 2022; Permenter *et al*., 2019). Heat stress induces complications such as acute lung injury and acute respiratory distress syndrome (ARDS) which are fatal and life-threatening (Sareh *et al*., 2010; Liu *et al.,* 2011).

Although heat stress negatively affects multiple organs in the body, some studies have investigated the effects of heat stress on the respiratory systems of animals. It has been found that the lungs of mice and baboons were severely damaged when their body temperature reached 42 °C due to heat stress (Bouchama *et al*., 2005; Liu *et al*., 2011). In mice, structural changes observed in the respiratory system include nasal mucosa lesions; characterised by sebaceous gland hyperplasia, tracheal lesions characterised by reduction of tracheal epithelial cells, a decrease of mucous epithelial cells in the bronchioles and alveolar expansion (Jin *et al*., 2011). Additionally, studies using birds displayed a loss of controlled movements, while rodents displayed significant amounts of hyperthermia (McKenchie & Wolf, 2019).

Cheshire (2016) and Bouchama *et al.,* (2017) state that the exact mechanism by which heat stress causes pathological changes remains unclear. However, it is known to interfere with DNA synthesis, transcription, mRNA processing, and translation. Numerous studies conducted on human and rat models show that the heat shock response is a precursor for the heat acclimation mechanism (Wheeler & Wong, 2006; Bouchama *et al.,* 2017). Also, alterations in gene expression and heat shock response generations triggered this response (Maloyan *et al*., 1999; Sareh *et al*., 2010).

1.1.7. Heat Acclimation

Heat acclimation is an adaptative physiological mechanism that improves the function of pre-existing structures, allowing organisms to better cope with environmental changes (Horowitz, 1998). This in turn increases their bodily temperature beyond their TNZ (Horowitz, 2002; Schwimmer *et al.,* 2004; Sawka *et al*., 1996). The process of heat acclimation involves the transfer of heat in order to lower the body's temperature and facilitate its cooling mechanism, thereby preventing heat-related illnesses and organ failure (Horowitz, 2002; Schwimmer *et*

al., 2004; Sawka *et al*., 1996). This adaptation reduces the heat stress experienced by endothermic organisms and in some cases, allows the body to expand its TNZ (Cole *et al*., 2023; Horowitz, 1998).

Phases of heat acclimation

Heat acclimation occurs in two phases: short-term heat acclimation (STHA) and long-term heat acclimation (LTHA) (Horowitz, 1998). Heat acclimation has long-lasting effects, and the response requires a significant amount of time to be successfully induced (Horowitz, 1998; Horowitz, 2002). STHA occurs within a period of 1 – 5 days and mostly relies on the autonomic nervous system to reduce the effects of heat stress on the body (Horowitz, 1998). A study conducted by Cole *et al.,* (2023), reported no physiological benefits on the third day of STHA, suggesting that more time is needed to induce effective heat acclimation responses. However; about 80% of cell and organ adaptations necessary for acclimation occur within this phase (Cole *et al.,* 2023). Additionally, in STHA, the signal is increased in order to redress any changes in the cell (Schwimmer *et al*., 2004). In contrast, LTHA occurs within 3 – 4 weeks, and because significant adaptations have occurred during STHA, the body attempts to achieve acclimatory homeostasis by lowering heart rate, metabolic activity, and increasing heat dissipation through sweating (Horowitz, 1998; Schwimmer *et al.,* 2004). Although there is a good understanding of physiological responses to heat, there remains a significant gap in the understanding of the biological or molecular response to this adaptive process (Sareh *et al.,* 2010).

While heat acclimation is induced to counter chronic heat exposure, heat shock response (HSR), in comparison, is a mechanism that is induced by acute heat exposure (Sawka *et al*., 1996; Horowitz, 1998). This process is regulated via the expression of heat shock proteins

(HSP) that protect the cell from damage (e.g., HSP27 and HSP70) (Sawka *et al*., 1996; Horowitz, 1998; Wheeler and Wong, 2006). This response is important because heat stress also causes protein denaturation and aggregation (Permenter *et al*., 2019). These proteins are degraded by proteosomes and lysosomes (Permenter *et al*., 2019). The HSR is crucial but needs to be kept at a minimum because excessive production of reactive oxygen species (ROS) produced by the mitochondria could lead to oxidative stress and death (Fedyaeva *et al*., 2014).

According to McEwan & Lasley (2002), animals are capable of adapting to stressors and returning to their normal state without any health issues. However, if the stressor is severe and prolonged, animals may not be able to adjust to the stressor and could develop serious health problems (Obernier & Baldwin, 2006). Ultimately, the intensity and duration of the stressor determine the speed at which animals can adapt and the extent of the physiological changes that may occur (Obernier & Baldwin, 2006).

Rats have a limited ability to regulate their body temperature due to the absence of sweat glands and panting mechanisms (Frohlich, 2020). Therefore, high temperatures can be very dangerous for rats. Thus, is recommended to keep rats in a temperature range of 18°C to 26°C (Frohlich, 2020). They are highly sensitive to temperature to the point that any temperature above 30°C can cause heat stress in rats, which can lead to heat stroke and respiratory complications (Frohlich, 2020).

1.1.8. Structure and Function of the Respiratory System of the Sprague Dawley Rat

The Origins of the Sprague Dawley Rat

Sprague Dawley (SD) Rats (*Rattus norvegicus*) are albino rats with an extended head and tail that were first bred by Robert S. Dawley at the Sprague-Dawley Animal Company in 1925

(Brower *et al*., 2015; Gileta *et al*., 2021; Gileta *et al*., 2022). Dawley bred SD rats using Wistar rats, wild stocks, and crossbreeds of those derived from laboratories (Brower *et al.*, 2015). Later, new species of SD rats were produced by Charles River Laboratories in the 1950s and by the Harlan Laboratory in the 1980s (Brower *et al.*, 2015). Due to being bred by different companies and the possibility of different breeding techniques being used, the genetic quality of SD rats may have evolved (Brower *et al*., 2015).

Sprague Dawley Rats as Models of Scientific Research

Sprague Dawley rats are used in biomedical research as animal models to aid in understanding human phenomena such as diabetes, cancer, and cardiovascular diseases (Brower *et al*., 2015; Gileta *et al*., 2022). This is due to the similar characteristics they share with human beings on an anatomical, genetic, and physiological level (Bryda, 2013). SD rats are bred with genetically diverse counterparts and produce various probabilities of disease manifestations that could lead to the development of multiple analyses and diverse therapeutic mediations (Brower *et al.,* 2015). Moreover, their small size, short life span, high sexual maturity and growth rate make it possible for many of them to be bred and used for scientific studies within a short space of time (Bryda, 2013; Gileta *et al*., 2022). Another advantage to the use of SD rats for scientific studies is the fact that they are cost-effective and provide ease of control in regulated environments to facilitate accuracy and repetition (Bryda, 2013; Gileta *et al.,* 2022).

The Respiratory System of the Sprague Dawley Rat

Sprague dawley rat lungs are pyramid-shaped organs joined to the trachea by the right and left bronchi (Bisgaard *et al*., 2002). The respiratory system of SD rats is divided into an upper and lower respiratory tract (Patwa & Shah, 2015). The respiratory system of SD rats is

categorised into two parts - upper and lower respiratory tract (Patwa & Shah, 2015). The nose, pharynx, and larynx make up the upper respiratory tract while the lower respiratory tract comprises the trachea and lungs, including the bronchi, bronchioles, alveolar ducts, and alveoli(Bisgaard *et al.,* 2002). The extrapulmonary airways, specifically the trachea, are lined by a pseudostratified ciliated columnar epithelium with goblet cells. Goblet cells are abundant in the trachea as compared to the intrapulmonary bronchus and respiratory epithelium (Mercer & Crapo, 1993; Suckow *et al.,* 2005). The respiratory epithelium also contains non-ciliated cells such as Clara, secretory, and brush cells (Miller *et al.,* 1993; Suckow *et al.,* 2005). In adult rats, the tracheal diameter measures approximately 1.6 to 1.7 mm, and its shape is supported by 18 to 24 C-shaped hyaline cartilage rings (Suckow *et al.,* 2005). The lower respiratory tract comprises five lobes, with four on the left (cranial, middle, accessory, and caudal) and one on the right. These lobes are further divided into lobules that consist of the bronchioles, thin interalveolar septa (IAS) walls, and clusters of alveoli (Kling, 2011; Khan & Lynch, 2018).

Bronchioles, IAS walls, and alveoli are collectively grouped as lung parenchyma that are involved in gaseous exchange (Suki *et al.,* 2011). Bronchioles are small passageways that extend from the bronchi and transport air from the trachea to the alveoli (Patwa & Shah, 2015; Suki *et al.,* 2011). They are lined by simple columnar to cuboidal epithelium (Suckow *et al.,* 2005). Alveoli are small, microscopic air sacs lined by type 1 and type 2 pneumocytes and located at the end of the bronchioles where gaseous exchange occurs (Pittman, 2011). IAS walls occur between two adjacent alveoli and are made up of a condensed network of capillaries and connective tissue fibres. It functions in strengthening the alveolar epithelium, aids by the regulation of blood flow, and assists in the transportation of oxygen and carbon

dioxide gases (Pittman, 2011). Functionally, the respiratory system can be subdivided into a conducting zone and a respiratory zone (Bisgaard *et al*., 2002). The conducting zone (the nose to bronchioles) is a passageway for respiratory gases such as oxygen and CO_2, while the respiratory zone (alveoli ducts to alveoli) is the site of gaseous exchange (Bisgaard *et al*., 2002). These structures are supported by collagen type II; contributing to the elasticity and flexibility of the treachea and bronchi; and smooth muscle (to keep all airways patent) allowing for adequate airflow for gas exchange and thermoregulation. SD rat lungs mainly function as a site of gaseous exchange in the alveolar region when air and blood are colonized across a large epithelial surface area that is highly permeable to gases (Knudsen & Ochs, 2018). This surface area is known as the blood-gas barrier (BGB) and is the passage site for respiratory gases in all vertebrates (Maina & West, 2005). Moreover, it is structured in such a way that it enables efficient gas exchange to take place (Maina & West, 2005).

Structure of the Pulmonary Blood-Gas Barrier

The pulmonary BGB is thin, strong, and made up of three layers: the alveolar epithelium, a fused basement membrane, and a capillary endothelium (Leiby et al., 2020; Maina & West 2005) (Fig. 1). The alveolar epithelium consists of Type I and Type II pneumocytes (Mason, 2006). Type I pneumocytes, which are squamous-shaped cells, make up 95% of the alveolar surface and form part of the BGB epithelial layer (Mason, 2006; Hakim & Usmani, 2014). Type II pneumocytes are a type of lung cell that are cuboidal in shape and cover around 5% of the alveolar surface in the lungs (Whitsett *et al.,* 2010; Mason, 2006). These cells are primarily responsible for producing and secreting surfactant, which helps to reduce surface tension within the alveoli and prevent the lungs from collapsing (Kazemi *et al.*, 2019; Brandt & Mandiga, 2020). The composition of the BGB includes flattened cells within both the alveolar

and endothelial layers, which collectively contribute to its thinness (Kazemi *et al.,* 2019; Mason, 2006; Brandt & Mandiga, 2020).

The thinness, strength, and large surface area of the barrier are crucial for efficient gaseous exchange (Makanya *et al*., 2013; Leiby *et al.,* 2020). This is because these characteristics allow for the diffusion of gases to occur efficiently and for the barrier to endure stress and maintain its integrity (Leiby *et al.,* 2020; West, 2009). According to West (2009), the strength of the barrier is attributed to the extracellular matrix that is found between the alveolar epithelium and capillary endothelium which has type IV collagen (Fig. 1).

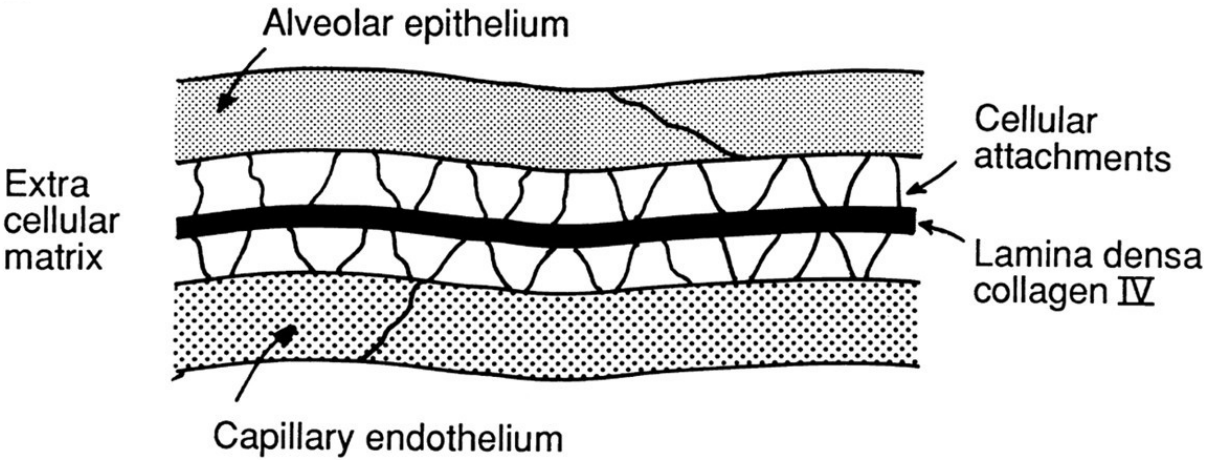


Figure 1: A diagram of the blood-gas barrier. The alveolar epithelium (top), extracellular matrix (middle), and capillary endothelium (bottom) are shown. The extracellular matrix between the alveolar epithelium and capillary endothelium, which contains type IV collagen, contributes to the strength of the BGB. Figure taken from West and Costello (1995).

Despite the strength of the BGB, there are instances when it can be compromised and unable to carry out its functions (West & Mathieu-Costello, 1999). Makanya *et al.,* (2013) reported that mechanical stress compromises the functionality of the human BGB. West and Costello

(1999) supported this by showing that an increase in stress on the walls of capillaries resulted in obstruction of endothelial and alveolar epithelial layers. Furthermore, it has been shown that the stress failure of pulmonary capillaries induces pulmonary oedema and alveolar haemorrhage (West & Costello, 1999). Maina & West (2003) studied the patterns that occurred when the BGB failed to withstand a stressor and summarised these into three alternatives:

1) Only the alveolar epithelial cell ruptures while the endothelium and basement membrane remain stable.
2) An endothelial cell ruptures while the rest remains stable.
3) The entire BGB ruptures and causes erythrocytes to enter the alveolar space.

1.2. Rationale for the Study

Climate change poses a threat to the conservation of biodiversity, ecosystems, human and animal life. The recent IPCC 2021 report projected that temperatures will rise beyond 1.5 °C – 2 °C in the next decade. Ultimately, it is anticipated that heatwaves will become more frequent, persistent, and intense in the coming years than previously anticipated (Meehl & Tebaldi, 2004). When this happens, will endotherms be able to cope with the rise in environmental temperatures and survive? That question prompted the purpose of this study which is to investigate whether endotherms will be able to acclimate when exposed to constant and high environmental temperatures.

Understanding the normal structure and function of the respiratory system in controlled environments will help in documenting the alterations in the lungs of those who are heat-stressed. The respiratory systems of rats are similar to those of humans, allowing for results

to be applicable across species (Suckow *et al.,* 2005). For the reasons stated above, the Sprague Dawley rat (*Rattus norvegicus*) model will be an ideal model organism to document the effects of chronic heat stress on the morphology of the respiratory system.

Exposure to acute heat stress can impair lung function and morphology and lead to heat-related illnesses. However, these changes are reversible upon cooling (Bouchama *et al.,* 2017). There is a gap in knowledge of the effects of chronic heat stress on the respiratory system. It is thus imperative to have more studies conducted on this topic. Proper knowledge and understanding of the effects of chronic heat on the lung morphology of Sprague Dawley rats could contribute to the advancement of data that will help bring solutions towards the conservation of species.

1.3. Aim and Objectives

Aim

To investigate the effects of chronic heat exposure on the architecture of the lungs of the Sprague Dawley rats.

Objectives

I. To document the gross morphology of the lung after chronic heat exposure.

II. To document the histology of the lung after chronic heat exposure, using multiple light microscopy staining techniques.

III. Use immunofluorescence microscopy to document the major structural components of the lungs after being exposed to chronic heat.

IV. To perform a histomorphometric analysis on alveolar size and interalveolar septa thickness, to observe changes during the respective temperatures using ImageJ analysis software (Schindelin *et al.,* 2012).

2. Material and Methods

2.1. Study animals

The animal research ethics committee (AREC) of the University of the Witwatersrand, granted a waiver for the conduct of this study (*Appendix 1)*. This study was part of an already approved project with the ethics clearance number (AREC 2019/04/19/C) (*Appendix 2)*. Twenty- four (24) adult Sprague Dawley rats (*Rattus novergicus domesticus)* aged between six to eight weeks were used in the study. They were housed at the Wits Research Animal Facility (WRAF) of the University of Witwatersrand.

2.2. Experimental Design

Twenty-four (n=24) adult rats were assigned individual numbers from one (1) to twenty-four (24) using a random number table. They were then divided and housed in three (3) different chambers: Chamber one (1) housed the control group (n = 8) that was exposed to standard reference ambient temperature (25 °C) (Haynes, 2014). Chambers two (2) and three (3) housed treatment groups B (n = 8) and C (n = 8) which were exposed to heat temperatures of 33 °C and 34 °C, respectively, for 24 hours over four (4) weeks (Fig. 3). Individual cages within the chambers housed one rat each, with unlimited access to food and water.

Each chamber's floor was covered with wet net material and watered each day (*as per* Washington State University's standard operating procedure, 2018) to maintain a relative humidity of 55 % ± 15 % (Fawcett & Rose, 2012). A hygrometer (PCE Instruments, Spain) was also used to measure the relative humidity in the chamber and to maintain the specified relative humidity experimental procedures. Maintaining a consistent humidity level within the chambers was crucial because low levels can result in impaired thermoregulation and

reduced intake of food (Fawcett & Rose, 2012). Moreover, high humidity may limit efficient evaporative heat loss (Fawcett & Rose, 2012).

Chamber description

Chambers used in this study had Infrared lamps (EuroLux, China) which were used to heat the chambers for groups B and C only. Each chamber had two (2) infrared lamps hung above the cages (Fig. 2), which were connected to a thermocouple (Maxim Integrated, USA) located inside the chamber's base. In this study, the thermocouples were used to regulate the temperature within each chamber. Each thermocouple was connected to its sensor circuit board. When the temperature in each chamber exceeded a specified fixed point (33 °C for group B and 34 °C for group C) the thermocouple would automatically detect this causing the circuit board to turn off the infrared lamps to avoid further temperature rise. Conversely; when the thermocouple detected a decrease in temperature below a specific temperature point (32 °C for group B and 33 °C for group C), it turned on the infrared lamps causing the environmental temperature to rise to their respective specific set points.

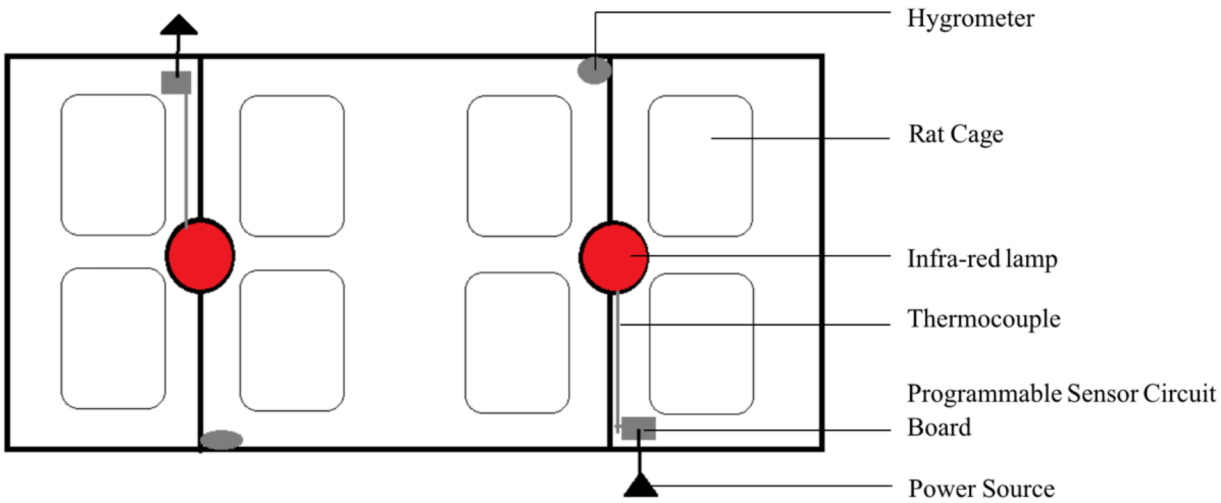


Figure 2: The diagram depicts a heat chamber that housed Sprague Dawley Rats in eight cages. It exhibits the connection between the infrared lamps (indicated by red circles) and the thermocouple that measures temperature. The programmable sensor circuit board regulates the temperature by controlling the infrared lamp's on and off switch based on the temperature change. The chamber also had a hygrometer to maintain the humidity level. (Figure courtesy: Stainbank-Minkova, 2022).

On day 28 following the rats' exposure to heat stress, they were euthanised using a weight-dependent (200 ml/kg) overdose of Sodium Pentobarbital (Kyro Laboratories, South Africa) administered via intraperitoneal injection (SANS:2008) (Fig. 4). This experiment was conducted at WRAF of the University of the Witwatersrand.

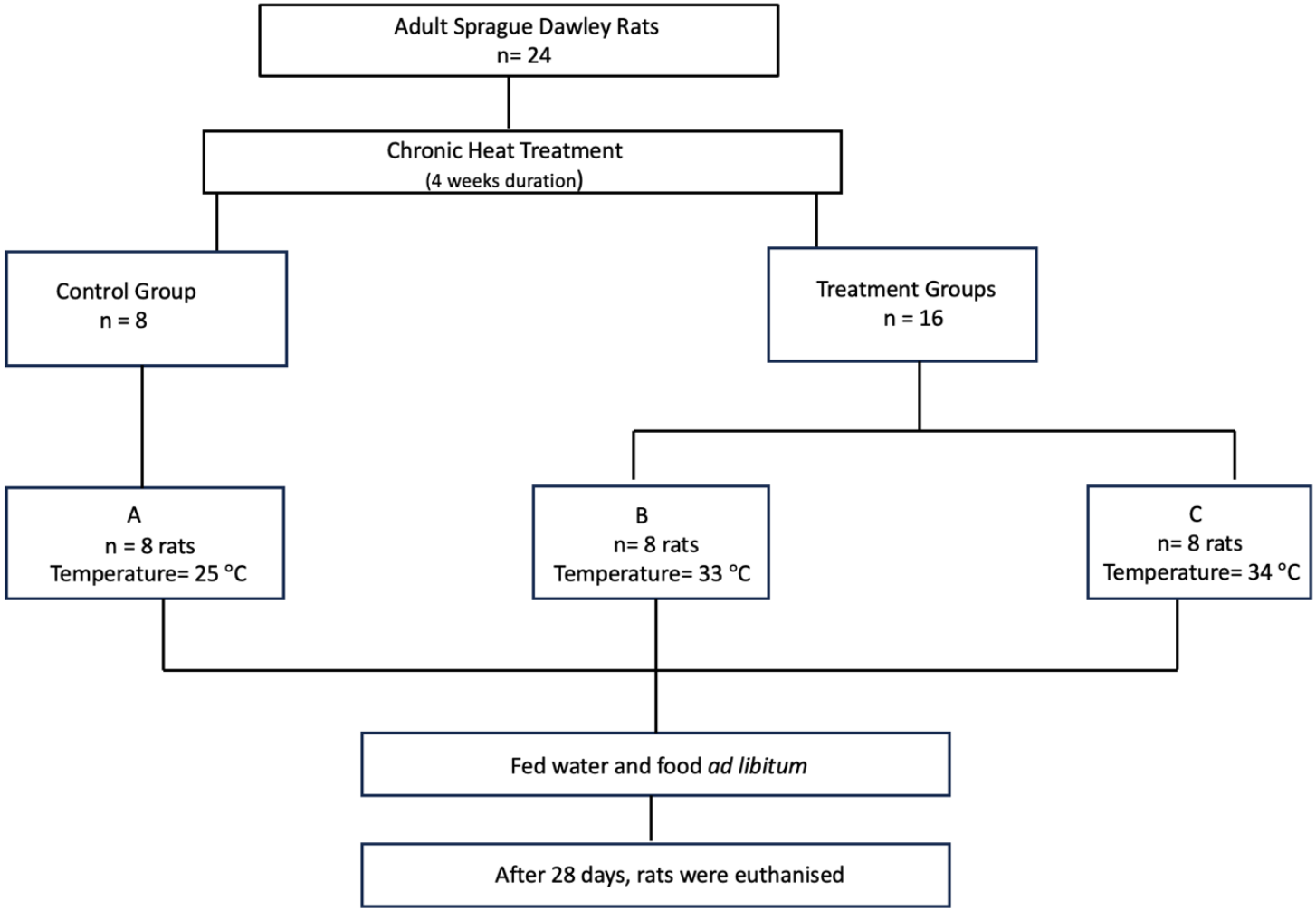


Figure 3: **An overview of the experimental design highlighting the workflow**. The Sprague Dawley rats were divided into three(3) groups and exposed to various temperatures for twenty-eight (28) days. They were housed in heated chambers and fed water and food daily. After 28 days, all rats were euthanised

2.3. Intra-tracheal Instillation

Following euthanasia, a small incision at the neck region of each rat was made. A cannula attached to a funnel was then inserted into the trachea and 10% buffered formalin (Merck KGaA, Darmstadt, Germany) was poured down, at a pressure of 30cm of water (Reddy, 2013). Once the lungs and extrapulmonary airways were filled with the fixative, the cannula was removed and the trachea was tied using a surgical ligature. Thereafter, the entire respiratory system was dissected from the thoracic cavity and submerged into the 10% buffered formalin for two (2) weeks before any further procedures.

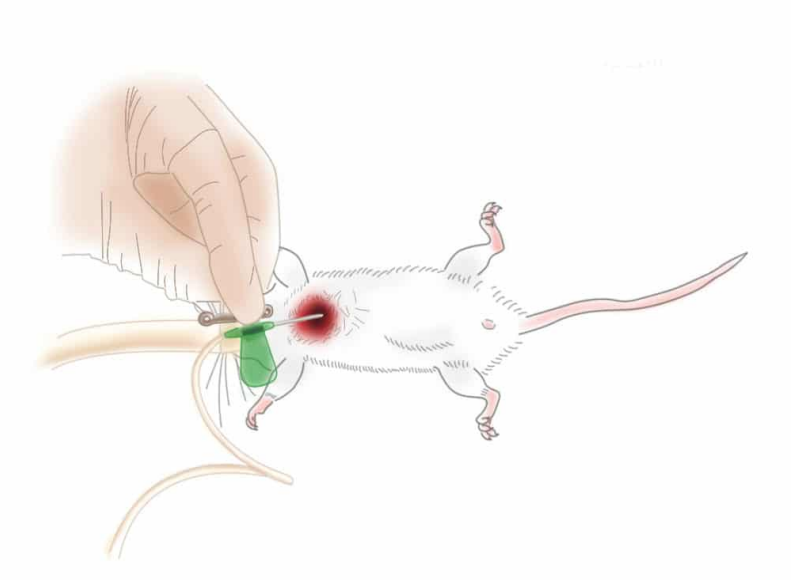


Figure 4: A Ventral view of the rat's gross morphology. This image depicts how the intratracheal instillation was done (https://bitly.ws/Ub6W).

2.4. Latex Casting

The purpose of creating latex casts was to express the gross morphology of the Sprague Dawley rat lung, in the best possible way, without damaging it and preserve the lung's natural structure (Reddy, 2013). An apparatus that has 2 independent closure valves (with attachments for disposable syringes) that attach to a single cannula was used to administer liquid latex to the lungs (Fig. 5). Firstly, an incision at the neck region was made and the cannula was inserted into the trachea. A ligature was then tied around the trachea (loosely) to secure the cannula in place. Two syringes were inserted into the respective valves of the apparatus; one syringe was empty and the other one was filled with a stock solution of 60% liquid latex (NJC adhesives, South Africa). The valve housing the latex syringe was closed and the other was opened. The lungs were then aspirated by extracting the air in the lungs. This was achieved by the suction created when pulling the plunger of an empty syringe repeatedly. After the aspiration of the lung, the first valve (initially empty valve) was closed and the valve housing the latex syringe was then opened. The liquid latex was then injected into the lung until pressure was perceived. Thereafter, the lungs were dissected out, submerged in water and housed in a fridge at ≈ 6 °C to set. After one (1) week, the casts were removed and all surrounding connective tissue was dissected and discarded.

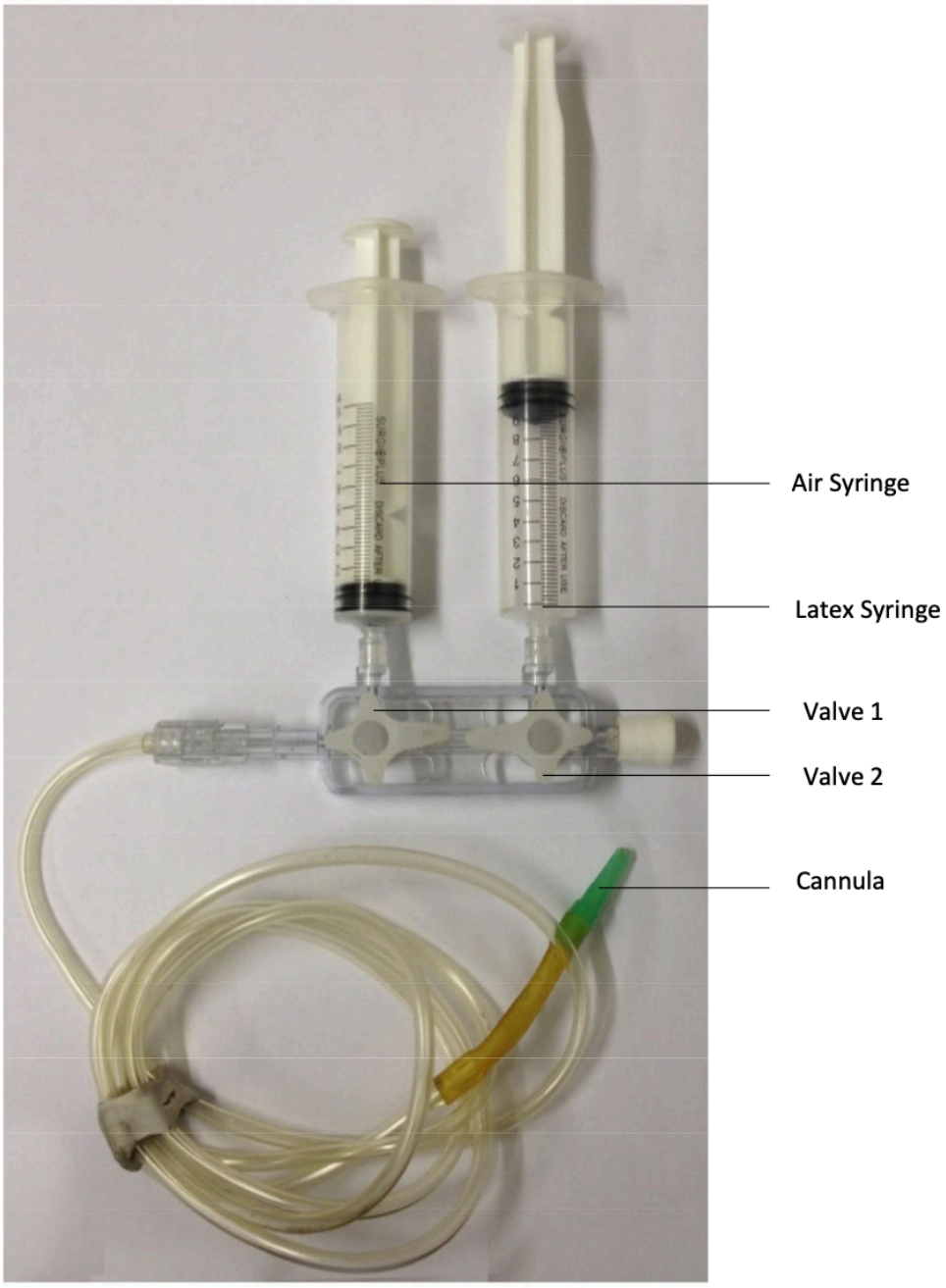


Figure 5: The equipment used for latex casting. The cannula was inserted and secured in the trachea in order to administer liquid latex to the lungs using a latex syringe**.** To aspirate the lung, an air syringe was used. Valves 1 and 2 ensured that the lung aspiration and latex injection were done independently (adapted from Reddy, 2013).

2.5. Gross Morphology

Following the submersion of the rat's lungs in 10% buffered formalin for two (2) weeks, the surrounding connective tissue on the lungs and extrapulmonary airways was removed. Following this, these lungs along with the latex casts were fully imaged using an Olympus MVX-10 Macro Zoom Microscope (Olympus, Japan) fitted with an Olympus DP-80 camera (Olympus, Japan). After this, the formalin fixed lung samples were dissected into dorsal and ventral halves along the sagittal plane.

2.6. Histology

Sampling of Lung Tissue

As described previously, the lungs were cut into dorsal and ventral halves along the sagittal plane (Fig. 6 A). The central points of the sampling regions were established by measuring the length of the respective halves of the lungs and dividing it into 3 sections, namely, cranial (Cr), middle (M) and caudal (Ca) (Fig. 6 B). These were the defining points to measure the breadth of the respective regions. The breadth of each of these regions was measured and divided by 2 to define a midpoint at which the respective sample tissues of 2 mm^3 were cut out (Fig. 6 C) This systematic region sampling (Reddy, 2013) helped to document the entire lung and all the changes (if any) that occurred due to heat stress.

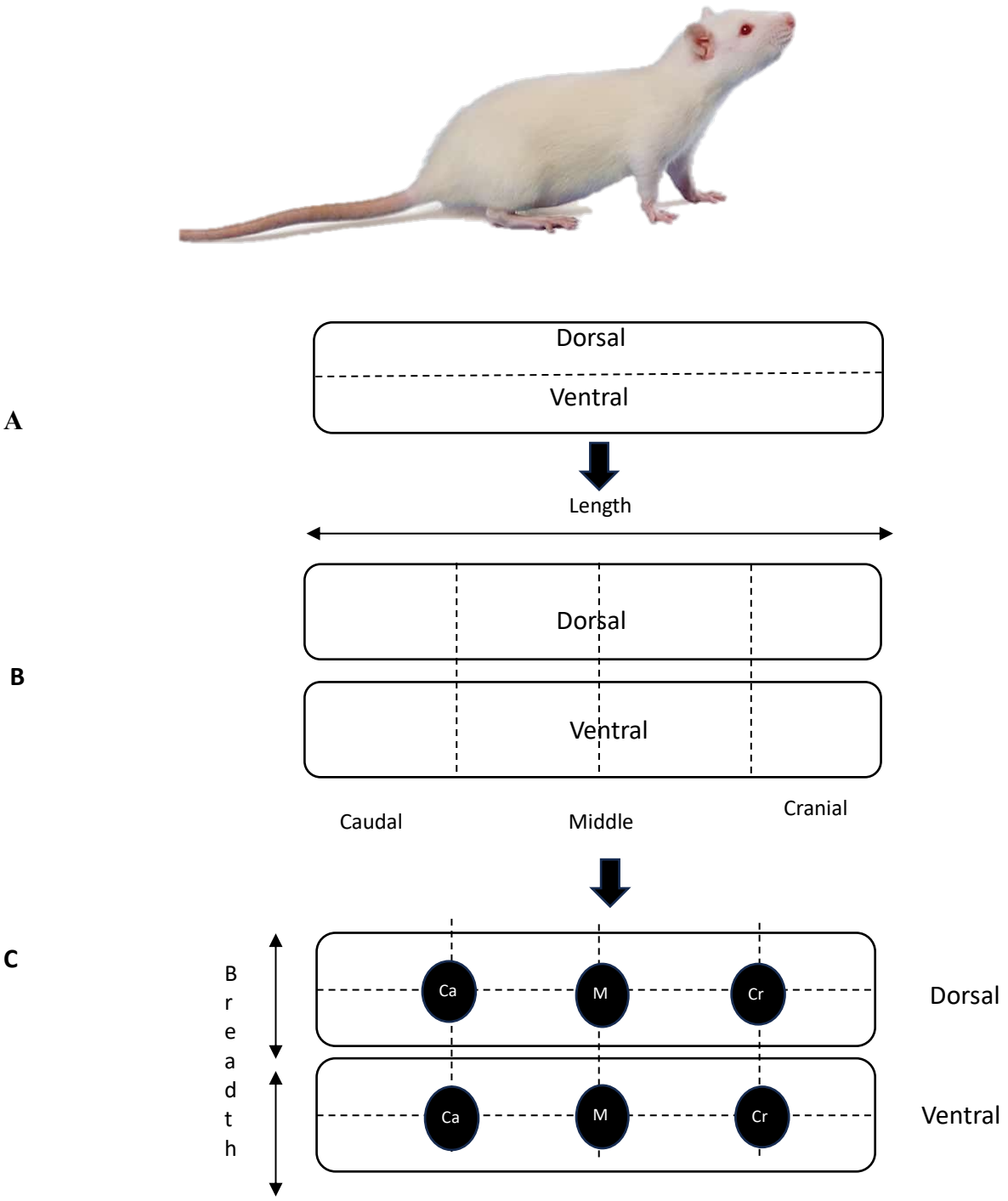


Figure 6: A diagram depicting the systematic regional sampling procedure for obtaining lung samples (adapted from Reddy, 2013). (A) The lung was cut into dorsal and ventral halves. (B) Three (3)defining regions were identified (Caudal, middle, and cranial) and (C) The midpoint was established.

2.7. Light Microscopy

Tissue Processing, Embedding and Sectioning of the Sampled Lung Tissue

Shortly after fine dissections and sampling, the samples were processed, sectioned, and stained in preparation for light microscopy. Sampled lung tissues were processed using an automated tissue processor (Shandon Citadel 2000, Thermo Fischer Scientific, UK) following standard techniques as outlined by Anderson & Bancroft (2002) at normal room temperature. The processor submerged tissue samples through 10% neutral buffered formalin, and an ascending series of alcohol changes overnight. Finally, tissues were submerged in two changes of Chloroform and paraffin wax *(Appendix 4*). After processing, the lung tissues were embedded in paraffin wax (VWR International LTD, Dublin, Ireland) on a Miles Scientific Tissue Tec® Cryo-console (Miles Scientific, USA) and left to solidify. Thereafter, embedded lung tissues were sectioned using a Leica 2035 Biocut rotary microtome (Leica Instruments GmbH, Germany). The sections were cut at a thickness of 5µm using disposable blades (Feather Safety Razor Co. Ltd., Japan). The cut sections were floated in a water bath set to 40 °C and then collected on microscope glass slides. All histological procedures were conducted at the School of Anatomical Sciences, University of Witwatersrand.

All the wax supporting and adhering the sectioned tissue to the glass slides was removed using xylene. This was followed by rehydrating them in a descending series of alcohol changes in preparation for the respective staining techniques.

Mayer's H&E Stain

A routine Mayer's Haematoxylin and Eosin (H&E) (Merck KGaA, Darmstadt, Germany) stain was used to look at the overall lung structure (Anderson & Bancroft, 2002). After staining, the sections were dehydrated in an ascending series of alcohol changes, cleared in xylene and coverslipped with Entellan mounting medium (Merck KGaA, Darmstadt, Germany). Haematoxylin stained the nuclei purple, while Eosin stained the cytoplasm and connective tissues pink-red (Chan, 2014) (*Appendix 5*).

Modified Verhoeff Elastic Van Gieson's stain

The Modified Verhoeff Elastic Van Gieson's stain (Merck KGaA, Darmstadt, Germany; Sigma-Aldrich, Saint Louis, USA) helped to differentiate between collagen and elastic fibres found in the lungs (Garvey *et al.,* 1991). After staining, sections were dehydrated in an ascending series of alcohol changes, cleared in xylene and coverslipped with Entellan mounting medium (Merck KGaA, Darmstadt, Germany). With this staining technique, the nuclei and elastic fibres stained black, collagen stained red, and muscle fibres stained yellow (Garvey *et al*., 1991) *(Appendix 6).*

Periodic Acid- Schiff Stain

The periodic acid Schiff (PAS)(Merck KGaA, Darmstadt, Germany) stain was used to stain polysaccharides (Dubray & Bezard, 1982). Shortly after staining, sections were dehydrated in an ascending series of alcohol changes, cleared in xylene and coverslipped with Entellan mounting medium (Merck KGaA, Darmstadt, Germany). The PAS stained the glycogen/mucus substances red-purplish and stained the nuclei blue (*Appendix 6).*

New Pentachrome stain

The New Pentachrome stain (Sigma-Aldrich, Saint Louis, USA) helped with tissue differentiation (Doello, 2014). After staining the sections, they were washed in running tap water and dehydrated in an ascending series of alcohol changes, cleared in xylene and coverslipped with Entellan mounting medium (Merck KGaA, Darmstadt, Germany) *(Appendix 8).* The new pentachrome stained.

- Collagen in red
- Sulphated mucopolysaccharides in violet,
- Muscle fibres in orange
- Cartilage in purple,
- Erythrocytes in yellow and nuclei in green (Doello, 2014).

RGB Trichrome stain

A novel Red-Green-Blue (RGB) trichrome stain (Sigma-Aldrich, Saint Louis, USA) was used to provide a clear tissue distinction by staining the main components of the lung tissue (Gaytan *et al.,* 2020). After staining the sections, they were dehydrated in two (2) changes of 100% alcohol, cleared in xylene, and coverslipped with Entellan mounting medium (Merck KGaA, Darmstadt, Germany). Collagen was stained by Sirius Red, Fast Green stained non-collagenous background proteins and Alcian Blue stained the primary components of the matrix ground material, glycosaminoglycans and proteoglycans (Gaytan *et al.,* 2020) (*Appendix 9*).

2.8. Immunofluorescence labelling procedures

Antibodies Optimisation

Immunofluorescence was used to identify specific structural components that are within the lung and are vital to the respiratory process. This technique removed any background that traditional light microscopy may cause, which has been known to obscure vital details or produce artefacts and will help to reliably localise and visualise the structural components of interest (Im *et al.,* 2019).

The lung parenchyma was labelled with anti-collagen II (anti-COL2) mouse monoclonal antibody (Abcam, UK) conjugated to Goat Anti-Mouse Alexa Fluor 594 antibody (Life Technologies, NL). The smooth muscle was labelled with anti-alpha-smooth muscle actin (anti-α-SMA) rabbit polyclonal antibody (Abcam, UK) conjugated to Goat Anti-Rabbit Alexa Fluor 488 antibody (Life Technologies, NL). Lastly, the sections were labelled with 4', 6-diamidino-2-phenylindole, dihydrochloride (DAPI) antibody (Abcam, UK) to label all nuclei that were present.

For all the aforementioned primary and secondary antibodies, positive and negative controls were conducted to test for reactivity, crosstalk/crossover, and optimisation of dilution factors. Optimisation of dilution factors for the experimental tissues was used, using the following controls: for anti-α-SMA, the rat colon tissue and human tonsil tissue were used as positive and negative controls, respectively. Furthermore, for anti-COL2, the human trachea and human heart were used as positive and negative controls, respectively. Human heart and tonsils were used as negative controls because they lack or minimally the proteins targeted by antibodies (e.g anti-COL2 and anti-α-SMA). Therefore, using the negative controls helped to distinguish a true signal from background noise or non specific binding.

Following this, an analysis of the sections was made and the following dilution factors were chosen, 1: 200 for anti-α-SMA 1:500 for anti-COL2, and 1:8000 for DAPI.

Immunofluorescence triple labelling

Slides with sections were dewaxed in xylene and rehydrated in a descending series of alcohols. Antigen retrieval was then done by immersing sections in a citrate buffer and placing them in a water bath (60 °C). The sections were removed from the water bath, allowed to cool and then washed in phosphate buffer solution (PBS). Thereafter, a circle was drawn around the sections with ImmEdge® PAP Pen (Vector Labs, USA) and then blocked with 10% normal goat serum at room temperature (25 °C). They were then incubated with anti-α-SMA (ab150301, Abcam, UK) antibody (1:200) overnight at 4 °C.

On the second day, sections were washed in PBS and incubated with goat anti-rabbit Alexa fluor 488 (Life Technologies, NL) (1:1000) at room temperature (25 °C) in a dark environment. Thereafter, sections were washed In PBS and incubated with anti-COL2 (ab88147, Abcam, UK) antibody (1:500) at 4°C overnight. On the last day, the sections were washed in PBS and incubated with goat anti-mouse Alexa fluor 594 (Life Technologies, NL) (1:1000) at room temperature (25 °C). Subsequently, they were washed with PBS and incubated with DAPI (Life Technologies, NL) (1:8000). Finally, sections were washed with PBS, coverslipped with fluoromount aqueous mounting medium (Sigma Aldrich, USA) and kept in the dark at 4°C until viewing (*Appendix 10).*

2.9. Microscopy

Following the staining and immunofluorescence procedures, outlined above, the resultant slides were viewed and imaged using an Olympus Microscope BX63 OFM (Olympus, Japan) fitted with an Olympus DP80 camera (Olympus, Japan) using CellSens Dimension software (v 1.12).

2.10. Morphometry

Micrographs of sections stained with Mayer's H&E were obtained using a 40x objective and used to measure alveolar size and septal thickness using Fiji version 1.53t image j analysis software (Schindelin *et al.*, 2012). By conducting a power analysis (SPSS® version 26), it was determined that four (4) measurements per micrograph were an adequate sample size for histomorphometry analysis using the random number table and a 100-point quadratic lattice. Alveolar size and septal thickness were measured using the freehand tool after the scale was calibrated. The longest diameter (major axis) was used to measure alveolar size, whilst septal thickness was determined by measuring the width of the interalveolar septum. A total of sixteen (16) measurements per group were taken for determination of both the alveolar size and septal thickness. The measurements were repeated three times and then the average was saved in a Microsoft Excel spread sheet (Microsoft Corporation, 2016).

2.11. Statistical analysis

The data was managed in Microsoft Excel 2016 (Microsoft Corporation, 2016) and analysed using SPSS® version 26 (SPSS Inc., Chicago). A Shapiro-Wilks test was used to test for normality ($p > 0.05$). Since the data was normally distributed, a One-way ANOVA (95% CI) was used to test differences between groups. Where significant differences were found, Dunnets and LSD post hoc tests were conducted. Dunnets post hoc test compared the treatment groups to the control group only, whilst the LSD post hoc test compared the difference between treatment groups and the control group. The data was reported as mean ± standard deviation.

3. Results

3.1. Gross Morphology

The lungs from group A (25 °C), which were fixed in formalin buffered solution, showed no abnormalities in their gross morphology (Fig. 7 A). Lungs from group B (33 °C) were fixed using latex casting and buffered formalin, resulting in a smoother surface with minor indentations (Fig. 7 B) and no other visible defects (Fig. 7 C). Group C (34 °C) had lighter-coloured lungs that still maintained their conical shape (Fig. 7 D).

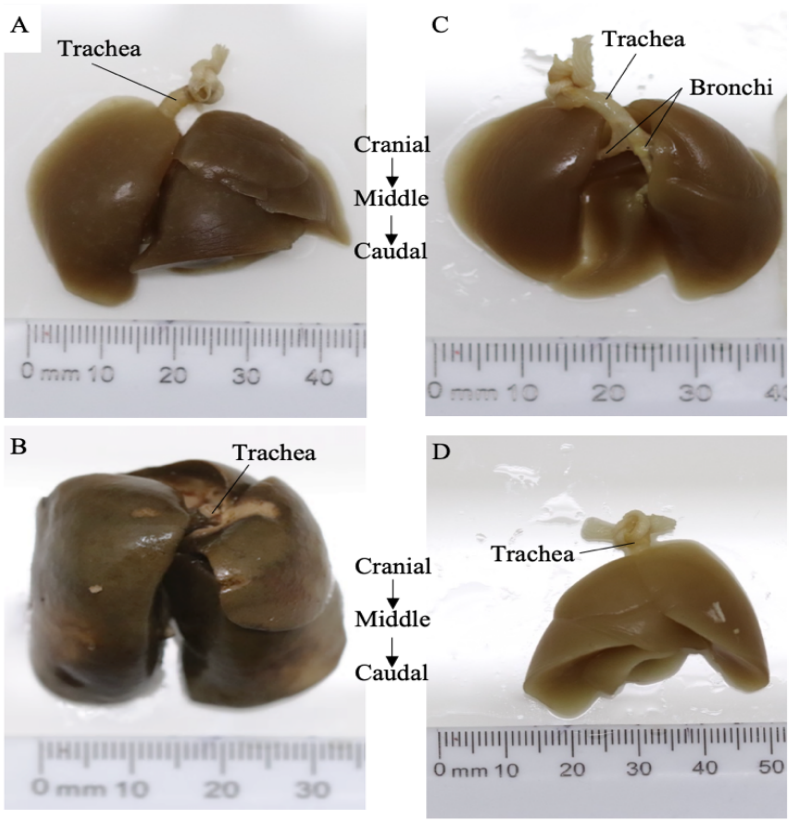


Figure 7: Images of the gross morphology of the lungs from control and treatment groups. (A) is a dorsal view image of a pair of lungs from group A (25 °C). The lungs appeared to be intact with no visible structural changes. (B) Group B (33 °C) displayed a lung fixed in a latex cast, it presented with a smooth surface with minor indentations and (C) the formalin-buffered fixed lung of group B (33 °C) showed no defects. (D) is an external ventral view image of a pair of lungs from group C (34 °C). The fixed lung appeared lighter in colour with no abnormalities observed.

3.2. Light Microscopy Analyses

Systematic region sampling – lung structure

Figure 8 shows micrographs of the sections displaying the division from the ventral cranial and dorsal cranial regions of the lung (Fig. 8 A-B). Additionally, it shows the ventral middle, dorsal middle (Fig. 8 C-D), ventral caudal and dorsal caudal regions (Fig. 8 E-F). These regions showed similar patterns of parenchymal division and structural distributions independent of the temperature with which the tissues were treated. This was the trend seen in all regional comparisons. The micrographs (Fig. 8) show all the structural components of the lung; enlarged bronchioles and blood vessels. Numerous alveoli, alveolar ducts, and alveolar sacs were notable. All these structures were free from any defects. The ventral caudal region will be used for all analyses.

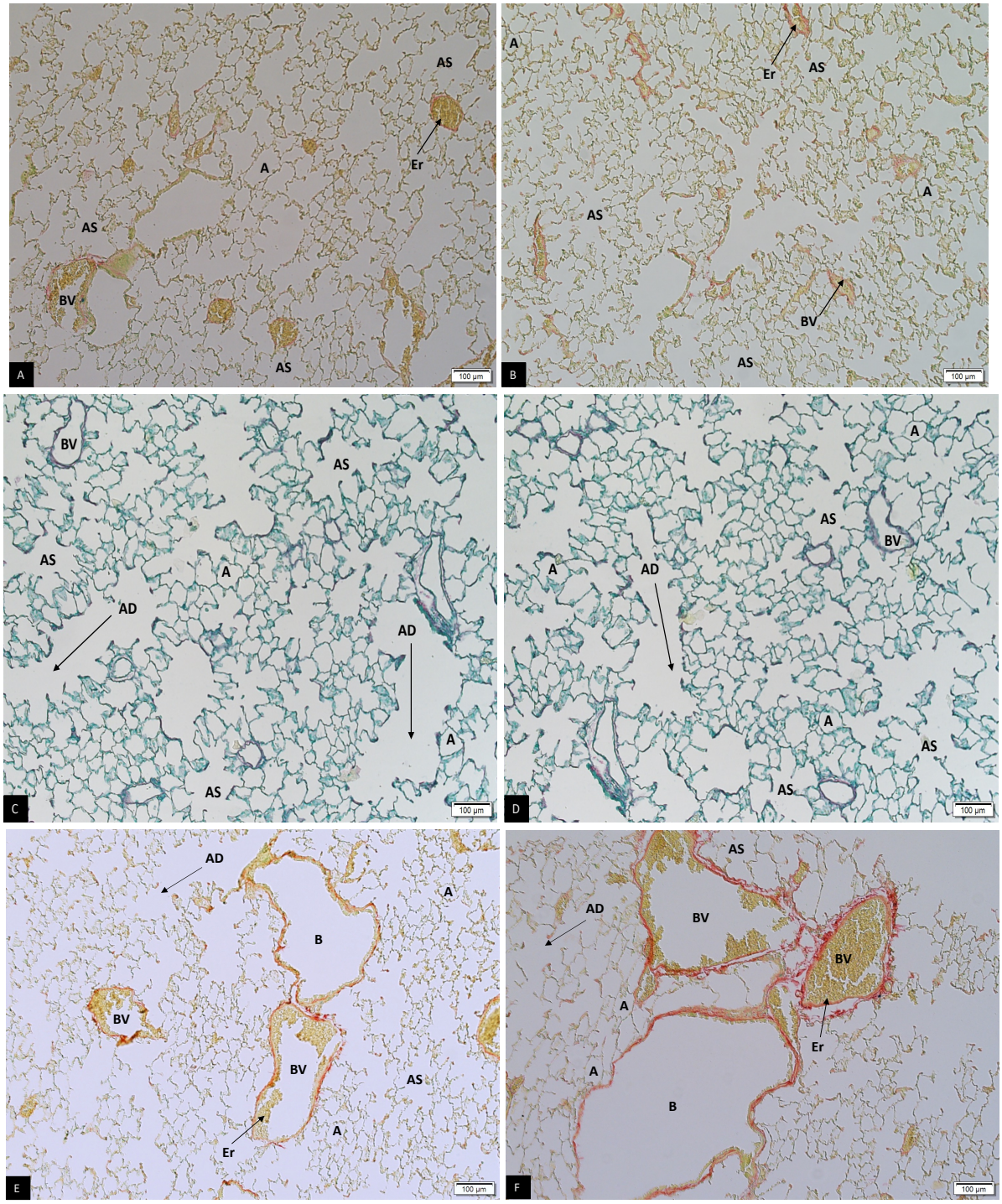


Figure 8: Micrographs of the new pentachrome and RGB stained sections displaying the subdivision of the lung structure from group A (25 °C). (A-B) represent sections from the ventral cranial and dorsal cranial regions. (C-D) represents sections from the ventral middle and dorsal middle regions. (E-F) represents sections from the ventral caudal and dorsal caudal regions. The parenchyma of all these regions was intact and well subdivided. There were numerous alveoli, large bronchioles, and blood vessels.

A=Alveolus; AS=Alveolar sac; AD = Alveolar duct; BV= Blood vessel; B=Bronchiole; Er= Erythrocytes

Scale bar = 100 µm

Lung parenchyma

The Mayer's H & E and new pentachrome stained sections of the lung parenchyma in group A (25 °C) presented no structural changes (Fig. 9 A-B). There were numerous alveoli with oval to circular shapes (Fig. 9 A-B). Additionally, the alveolar ducts were progressively branching and narrowing as they approached the alveolar sacs. These sacs were well opened and no defects were observed (Fig. 9 A-B). The bronchial epithelium had high adherence to the basement membrane and its integrity was well intact (Fig. 9 A-B).

In group B (33 °C), there were apparent structural differences compared to group A (25 °C) (Fig. 9 C-D). The alveoli were numerous and round with wider lumens (Fig. 9 C-D). With regards to the bronchioles, they were bigger and expanded across the lung parenchyma (Fig. 9 C-D). Moreover, the pseudostratified columnar epithelium was severely peeling off (Fig. 9 C-D). Clusters of lymphocytes known as Bronchus associated lymphoid tissue (BALT) were also present outside the bronchioles (Fig. 9 C-D). Lastly, the blood vessels were larger with smooth muscle hypertrophy (Fig. 9 C-D).

The lung parenchyma of group C (34 °C) was severely damaged (Fig. 9 E-F). The alveoli appeared disintegrated with wider lumens, containing an excessive amount of surfactant (Fig. 9 E-F) and thus larger alveolar spaces were evident (Fig. 9 E-F). Moreover, the blood vessels had smooth muscle hypertrophy, as was seen in group B (33 °C). The bronchioles were enlarged with excessive collagen deposition and BALT around them. The loss of epithelial integrity was notable. This is seen by the loss of epithelial adherence to the basement membrane (Fig. 9 E-F).

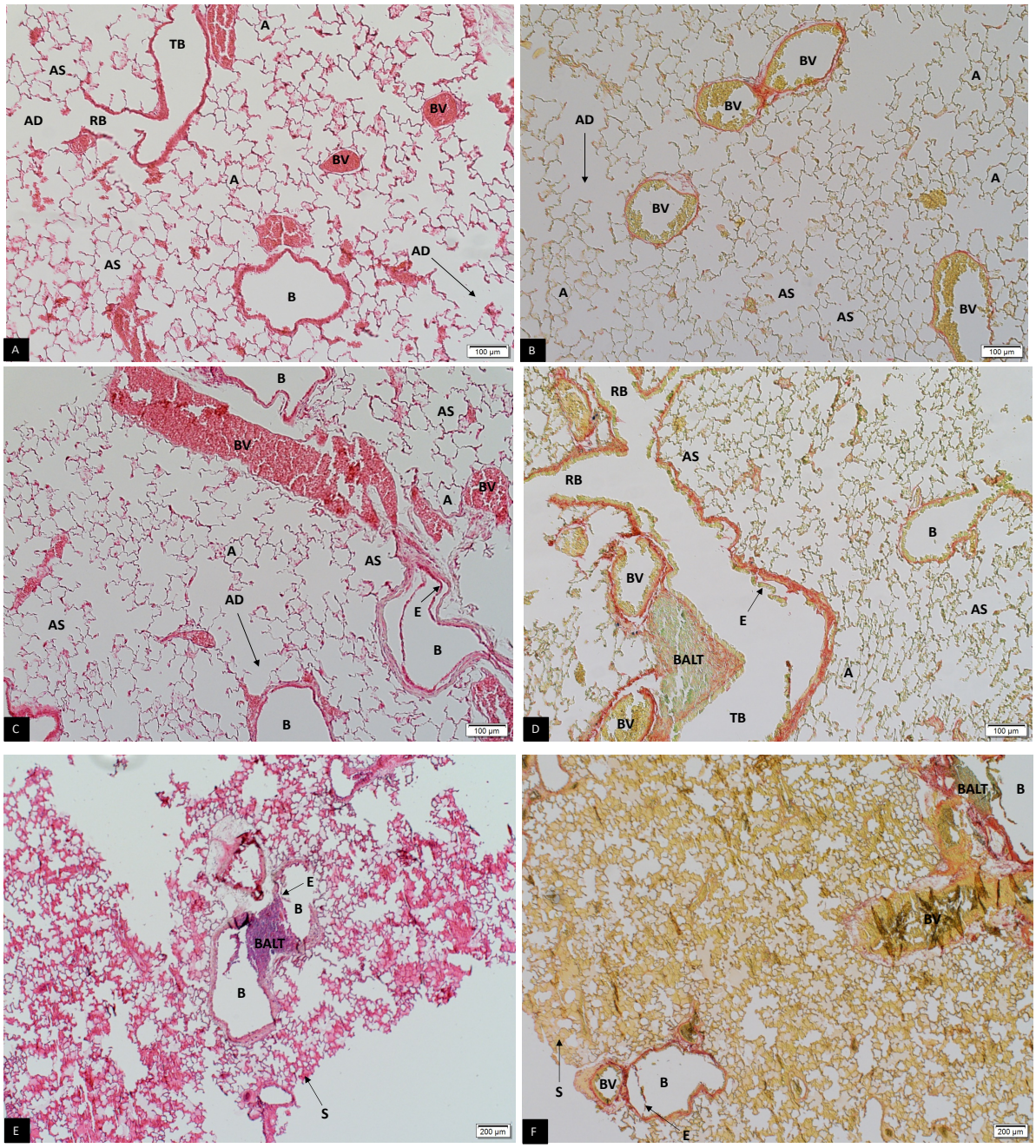


Figure 9: Micrographs of Mayers H&E and new pentachrome stained sections of the lung parenchyma from the control and treatment groups. (A-B) Group A (25 °C), displayed an intact lung parenchyma which has numerous alveoli, alveolar ducts, blood vessels and different types of bronchioles that are free from defects. (C-D) Group B (33 °C) had numerous alveoli with wider lumens. The blood vessels were larger and had smooth muscle hypertrophy. Bronchioles were larger and the loss of epithelium integrity was notable. BALT was also present along the bronchiole. (E-F) Group C (34 °C) had a severely damaged lung parenchyma. There was excessive surfactant in the alveoli

A=Alveolus; AS=Alveolar sac; AD=Alveolar duct; BV= Blood vessel; B=Bronchiole; BALT=Bronchiole associated lymphoid tissue; E=Epithelium; RB=Respiratory bronchiole; TB=Terminal bronchiole; S= Surfactant; Scale bar = 100 µm

Bronchioles

The bronchioles in group A (25 °C) had intact epithelium with Clara cells (Fig. 10 A-B) compared to group B (33 °C) and C (34 °C). The collagen around the bronchioles appeared to be thin in comparison to the bronchioles of groups B (33 °C) and C (34 °C) (Fig. 10 A-B).

In group B (33 °C), the pseudostratified ciliated columnar epithelium of the bronchiole was severely detached from the underlying basement membrane (Fig. 10 C-D). Besides this damage, they were numerous and larger (Fig. 10 C-D). There was also excessive collagen, connective tissue (Fig. 10 C-D), and BALT deposition (Fig. 11 C-D) around the bronchioles.

Similarly, in group C (34 °C) the pseudostratified ciliated columnar epithelium was peeling off (Fig. 10 E-F). There was also excessive collagen, connective tissue (Fig. 10 E-F), and BALT (Fig. 11 E-F) deposition around the bronchioles compared to group B (33 °C).

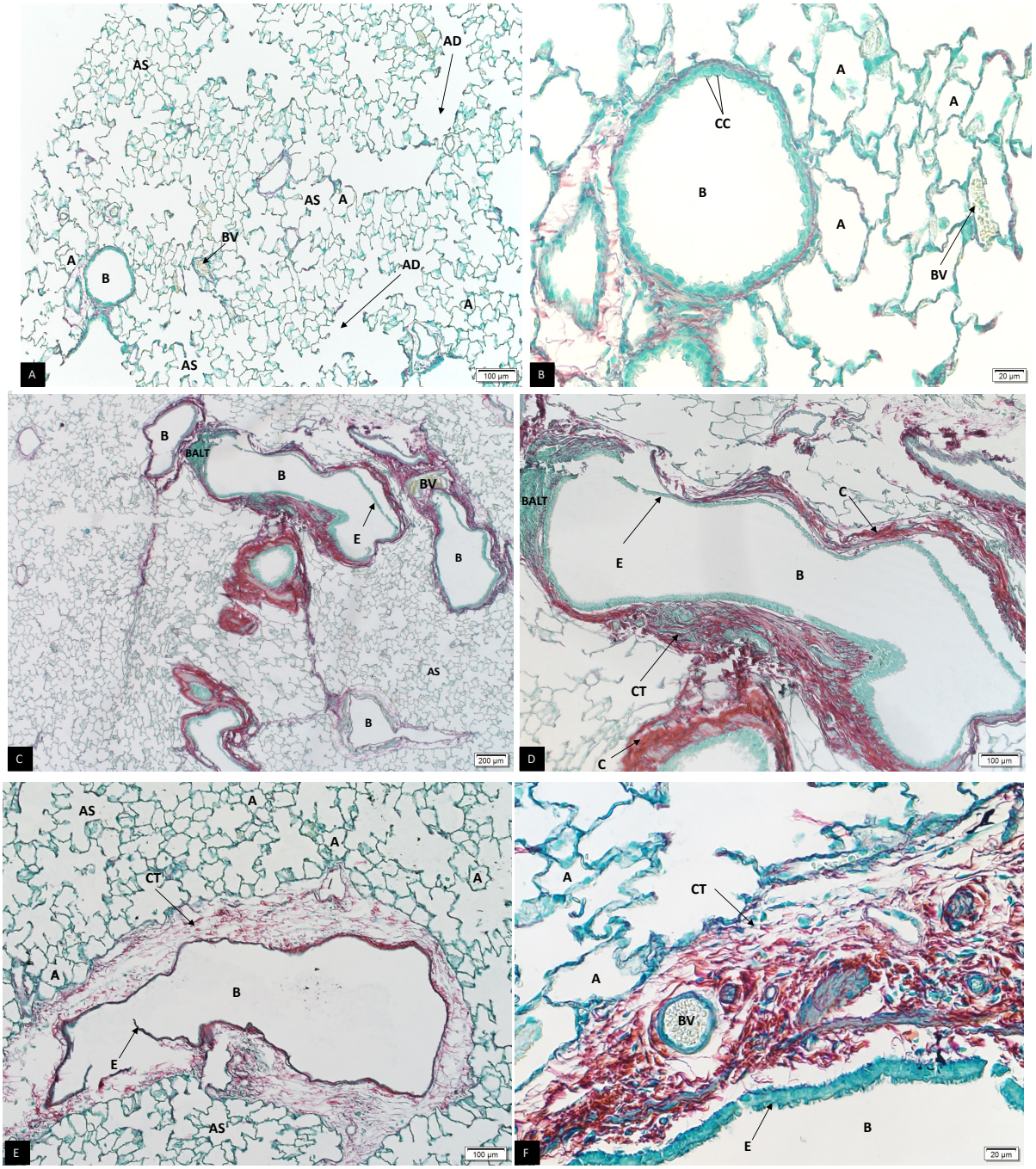


Figure 10: Micrographs of RGB trichrome stained sections of the lung displaying bronchioles from the control and treatment groups. (A-B) group A (25 °C) had bronchioles with intact epithelium with clara cells. (C-D) Group B (33 °C) had larger bronchioles with loss of ciliated pseudostratified columnar epithelial integrity. Increased collagen deposition is also notable. (E-F) Group C (34 °C), show severe loss of ciliated pseudostratified ciliated columnar epithelial integrity. Excessive collagen and connective tissue deposition were also visible.

A=Alveolus; AS=Alveolar sac; AD=Alveolar duct; BV=Blood vessel; B=Bronchiole; BALT=Bronchiole associated lymphoid tissue; CC= Clara cells; C=Collagen; CT=Connective Tissue; E= Epithelium. Scale bar = 100 µm

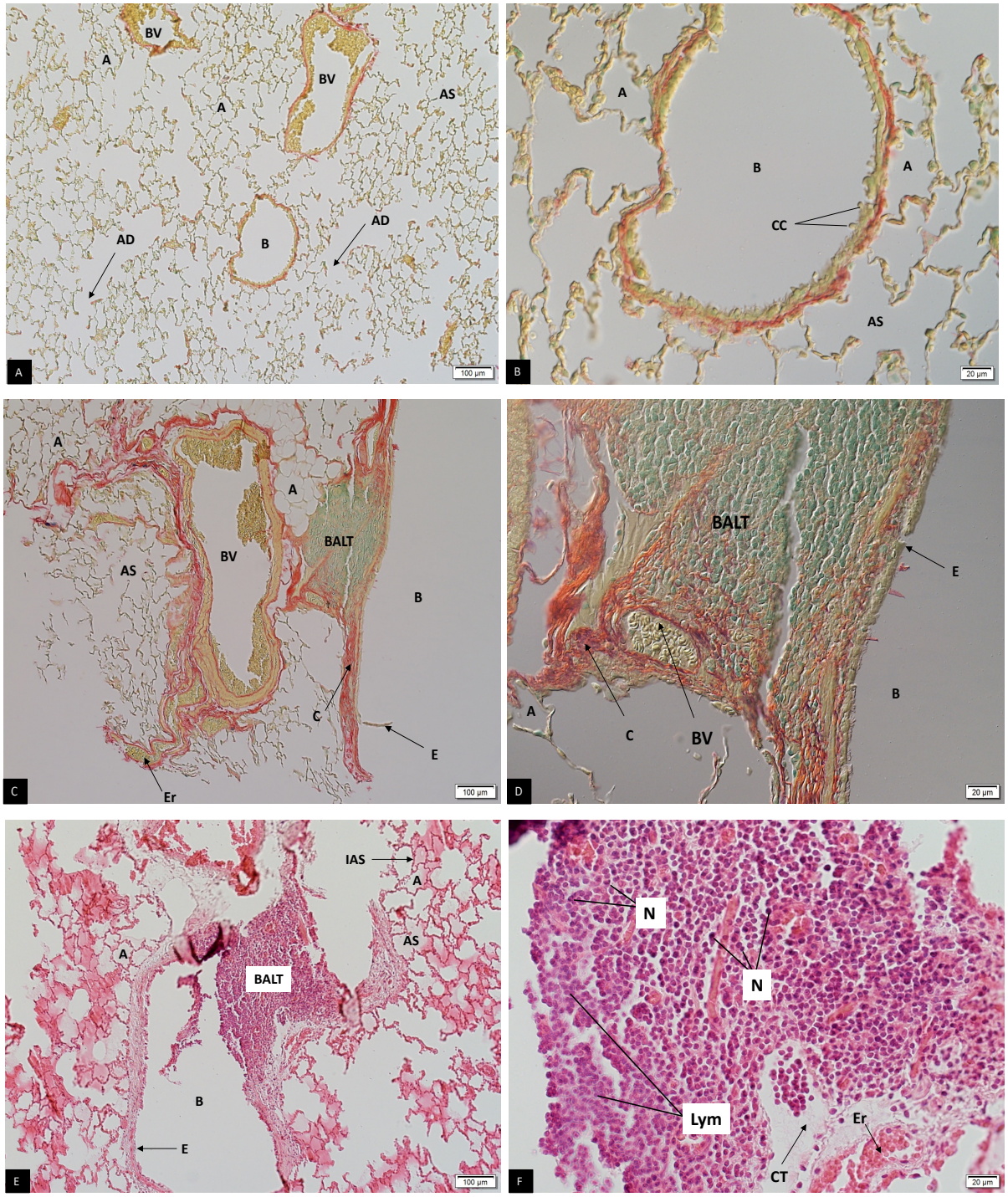


Figure 11: Micrographs of new pentachrome and Mayer's H&E-stained sections of the bronchiole from the control and treatment groups. (A-B) Group A (25 °C) shows the absence of BALT. (C-D) Group B (33 °C) shows the presence of BALT outside the bronchiole and collagen deposition. (E-F) Group C (34 °C) shows large clusters of numerous cells that make up BALT.

A=Alveolus; AS=Alveolar sac; AD=Alveolar duct; BV=Blood vessel; BALT=Bronchiole associated lymphoid tissue; E= Epithelium; CC=Clara cells; IAS=Interalveolarsepta; Lym=Lymphocytes; N=Neutrophils; Er=Erythrocytes; Scale bar = 20 and 100 µm

Alveoli

Lung parenchyma is divided into numerous alveoli by thin IAS. (Fig. 12 A-B). Sections stained with Mayers H&E from group A (25 °C) showed numerous, oval shaped alveoli with thinner IAS compared to groups B (33 °C) and C (34 °C) (Fig. 12 A-B). The RGB trichrome-stained sections also showed thin collagen deposition around the alveoli and IAS (Fig. 13 A-B). Overall, the alveoli were free from any damage or abnormalities.

In group B (33 °C), the alveoli were less round/oval and had wider lumens (Fig. 12 C-D and Fig. 13 C-D). There was excessive infiltration of erythrocytes in the alveoli (Fig. 12 D and Fig. 13 C). Although majority of the IAS appeared thin, fewer alveoli were seen to have thicker IAS when compared with group A (25 °C) (Fig. 12 D and Fig. 13 C-D). Numerous type II Pneumocytes were also present around the alveoli and IAS wall (Fig. 12 D). Moreover, there was an increase in the collagen deposition around the alveoli in comparison to group A (25 °C) (Fig. 13 D).

The alveoli in group C (34 °C) appeared larger (Fig. 12 E-F), and there was even the presence of large alveolar space (Fig. 14 A). Pulmonary oedema and excessive surfactant were notable in the lumens of the alveoli (Fig. 12 E-F). Moreover, there was increased collagen deposition and IAS thickness compared to group A (25 °C) and group B (33 °C) (Fig. 13 E-F). Correlative to group B (33 °C), there was the presence of immune cells around the alveoli and IAS. Interestingly, where there were immune cells, the collagen deposition was more excessive (Fig. 13 F).

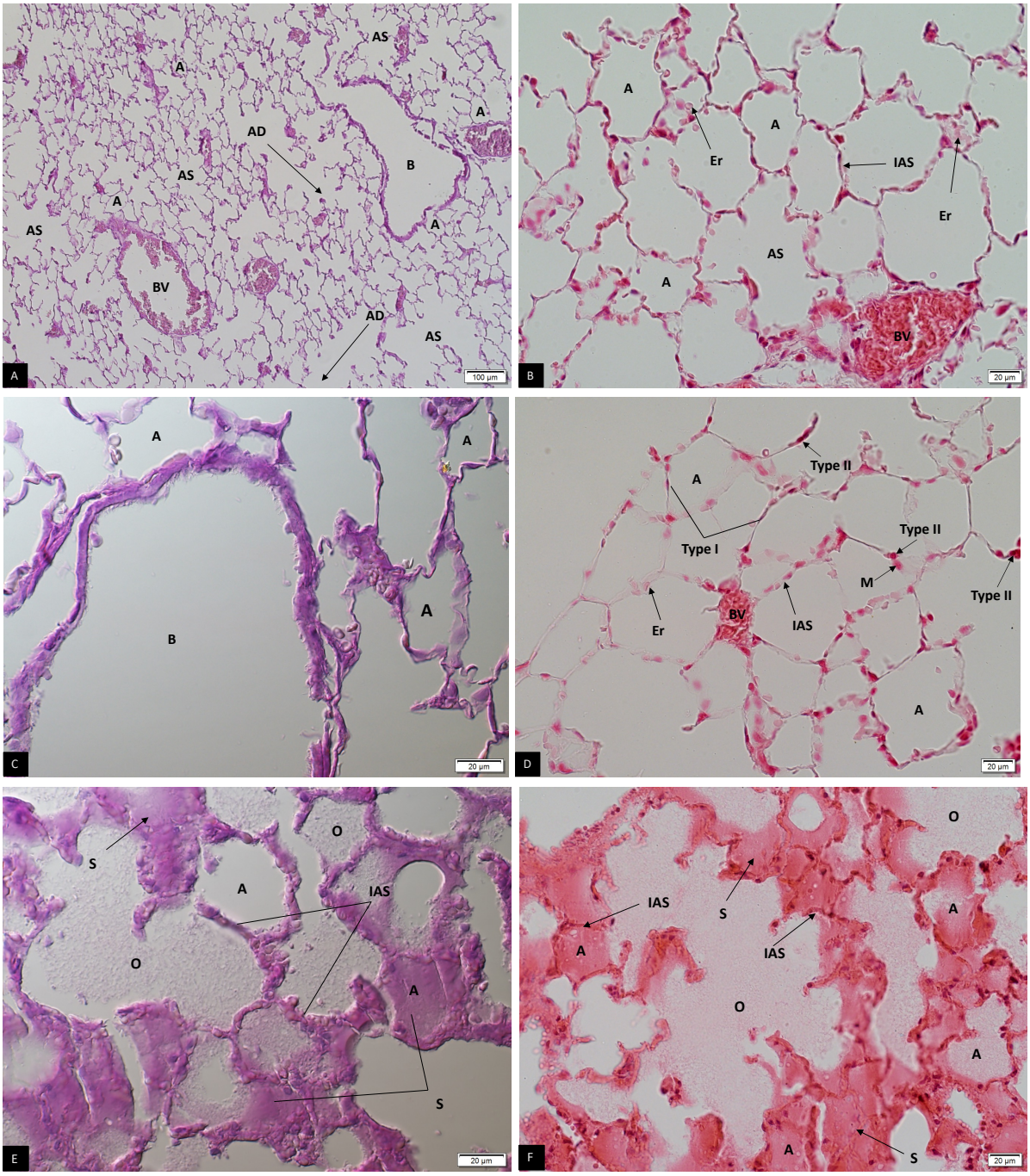


Figure 12: Micrographs of Mayer's H&E and PAS-stained sections displaying the alveoli architecture from the control and treatment groups. (A-B) Group A (25 °C) had numerous round alveoli and thin IAS. (C-D) Group B (33 °C) had wider alveoli with erythrocyte infiltration. There were thicker IAS and the presence of macrophages, type I and II pneumocytes. (E-F) Group C (34 °C) had larger alveoli that had oedema and excessive surfactant. The IAS were thicker.

A=Alveolus; IAS=Interalveolar septa; B=Bronchioles; BV=Blood vessel; Er=Erythrocytes; S=Surfactant; Type I=Type I Pneumocytes; Type II=Type II Pneumocytes; M=Macrophages; O=Oedema;
Scale bar = 20 µm

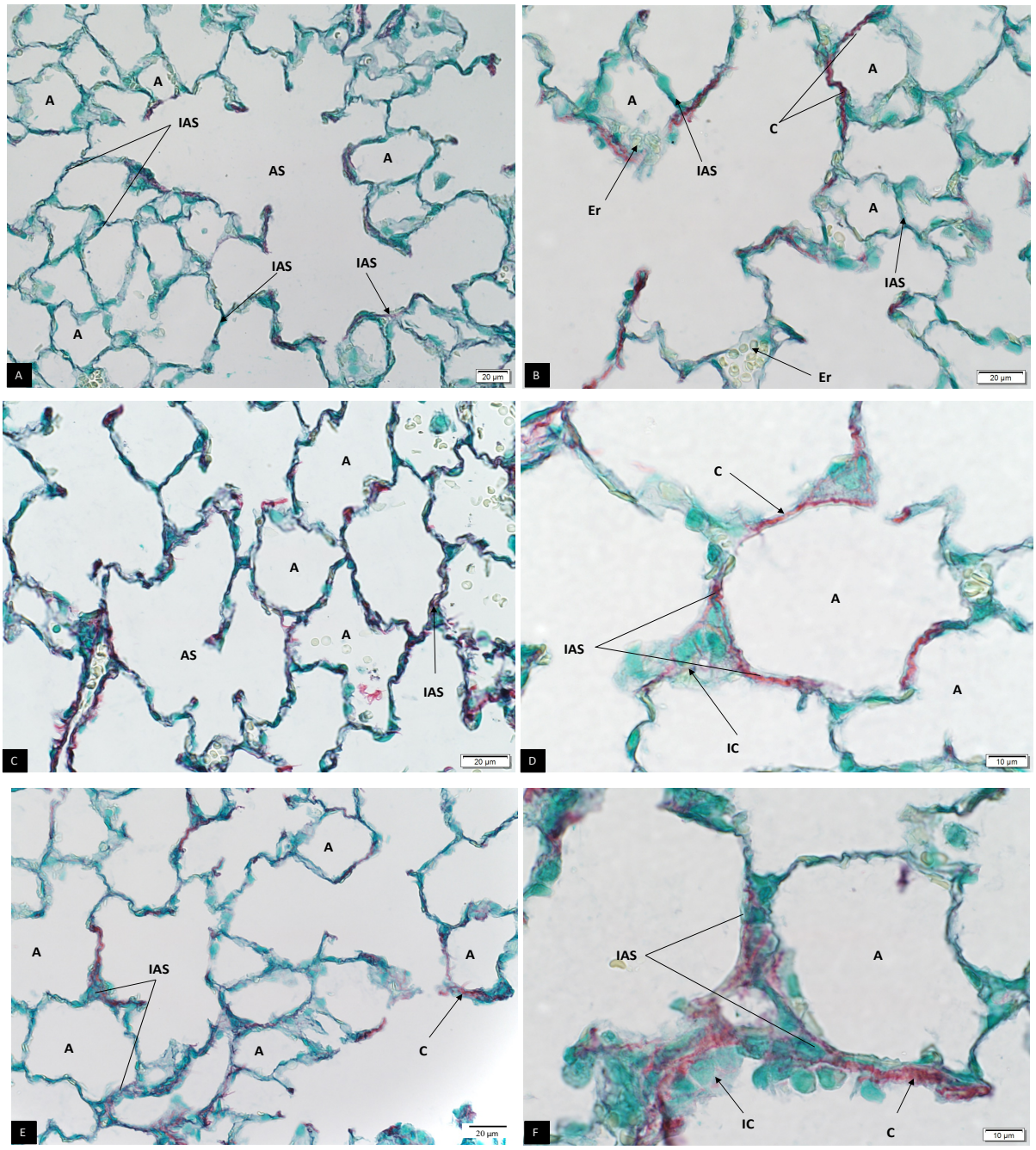


Figure 13: Micrographs of RGB trichrome stained sections displaying collagen deposition around the alveoli from control and treatment groups. (A-B) Group A (25 °C) had numerous alveoli with the presence of erythrocytes in some alveoli. Collagen deposition around the alveoli and IAS was notable. (C-D) Group B (33 °C) had oval-shaped alveoli with wider lumens. There was increased collagen deposition around the alveoli. Thicker IAS infiltrated by immune cells were also notable. (E-F) Group C (34 °C) had larger alveoli with wider lumens. There was excessive collagen deposition around the alveoli and IAS. The IAS were much thicker and infiltrated by immune cells.

A=Alveolus; AS=Alveolar sac; IAS=Interalveolar septa; Er=Erythrocytes; IC=Immune cells; C=Collagen; Scale bar = 20 µm

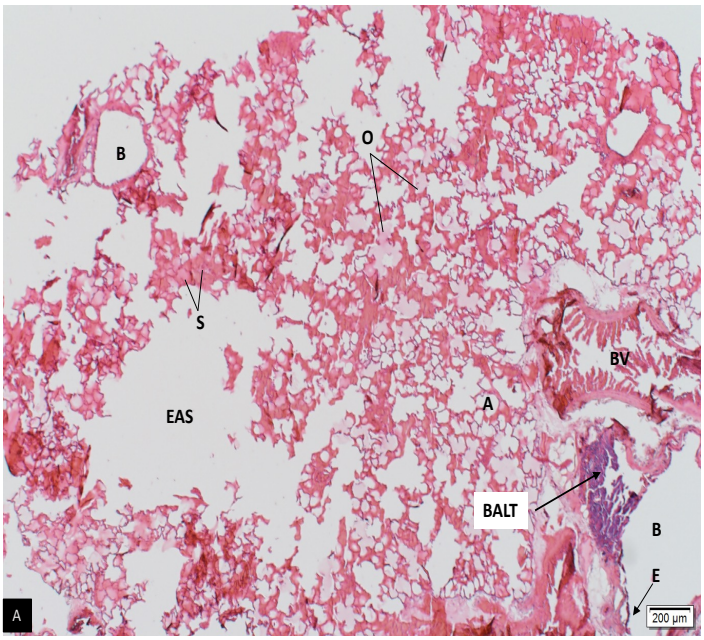


Figure 14: Micrographs of Mayer's H&E-stained section displaying enlarged alveolar space from treatment group C (34 °C). (A) The lung parenchyma appears to be severely damaged. There was pulmonary oedema and excessive surfactant in the alveolar space**.**

A=Alveolus; B=Bronchiole; BALT=Bronchus associated lymphoid tissue; BV=Blood vessel; E= Epithelium; EAS = Enlarged alveolar space; O= Oedema; S= Surfactant;

Scale bar = 200 µm

Blood vessels

Sections of blood vessels from control and treatment groups were stained with the Modified Verhoeff Elastic von Gieson stain. The blood vessels in group A (25 °C) had thin tunica externa with few elastic and collagen fibres compared to group B (33 °C) and C (34 °C) (Fig. 15 A-B).

In group B (33 °C), the blood vessel (artery) had hypertrophied tunica media with prominent elastic fibres known as internal and external lamina (Fig. 15 D). In addition to this, increased collagen deposition around the artery was notable (Fig. 15 C-D).

The blood vessels in group C (34 °C) were more pronounced with smooth muscle hypertrophy. They also had more prominent elastic fibres which appeared darker. (Fig. 15 E-F). Additionally, excessive collagen and fluid cuffs deposition were observed between the bronchioles and blood vessels (Fig. 15 E-F).

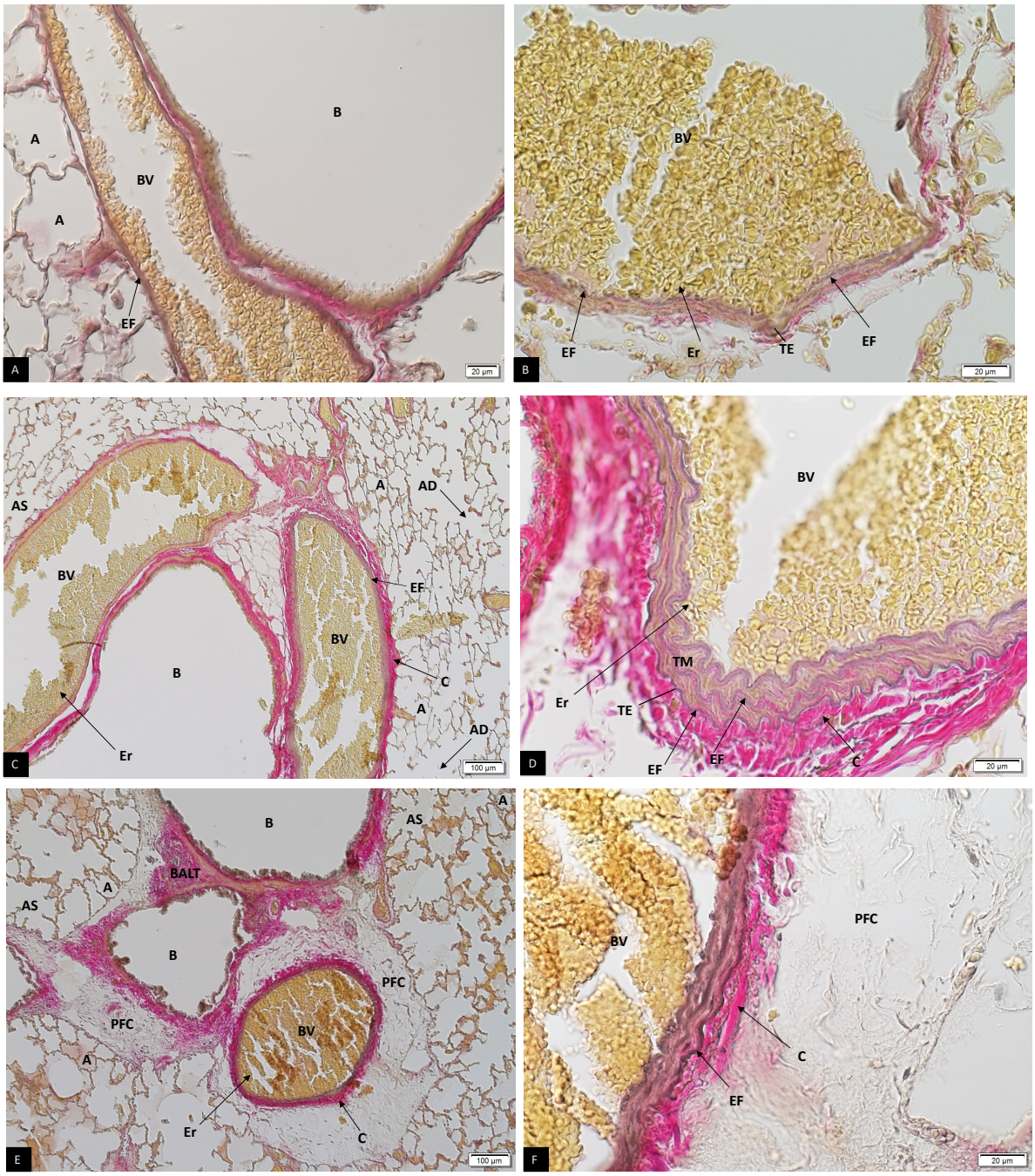


Figure 15: Micrographs of Modified Verfhoeff van Gieson stained sections of the blood vessels from the control and treatment groups. (A-B) Group A (25 °C) had blood vessels with thin tunica externa with few elastic and collagen fibres. (C-D) Group B (33 °C) had larger blood vessels with smooth muscle hypertrophy. Prominent elastic fibres in the tunica media of blood vessels were visible (E-F) Group C (34 °C) had blood vessels with more prominent elastic fibres, increased collagen and perivascular fluid cuffs depositions were also visible.

A=Alveolus; AS= Alveolar sac; AD= Alveolar duct; BV= Blood vessel; B= Bronchiole; BALT= Bronchus associated lymphoid tissue; C=Collagen; EF = Elastic fibres; Er= Erythrocytes; PFC= Perivascular fluid cuffs; TE= Tunica externa; TM= Tunica media;

Scale bar = 20 and 100 µm

Table 1: Summary of the lung structural alterations and observation after chronic heat exposure

	Group A (25 °C)	**Group B (33 °C)**	**Group C (34 °C)**
Lung Parenchyma	• Intact lung parenchyma	• Semi intact lung parenchyma	• Damaged lung parenchyma
Structural changes	• No abnormalities were observed.	• Large alveoli • Thick interalveolar Septa • Large blood vessels • Smooth muscle hypertrophy • Large bronchioles • BALT • Loss of epithelium integrity in the bronchioles • Prominent elastic fibres • Excessive collagen deposition (than all groups)	• Larger alveoli • Thicker interalveolar Septa • Large blood vessels • Smooth muscle hypertrophy • Large bronchioles • BALT • Loss of epithelium integrity in the bronchioles • More prominent elastic fibres • Increased collagen deposition • Connective tissue deposition • Oedema • Excessive PAS positive surfactant

3.3. Histomorphometry

There was a significant difference in the mean alveolar size between the 3 groups. A one way ANOVA was conducted to check this, resulting in P < 0.001 (table 2). Dunnett's Post hoc tests showed that the mean alveoli size was significantly smaller in group A (25 °C) (mean = 3.64µm ±0.18) compared to group B (33 °C) (mean = 4.22 µm ±0.14) and C (34 °C) (mean = 4.59µm ±0.17) (Fig. 16). Similarly, LSD post hoc test showed that the mean alveoli size in group B (33 °C) was significantly smaller than in group C (34 °C) (Fig. 16).

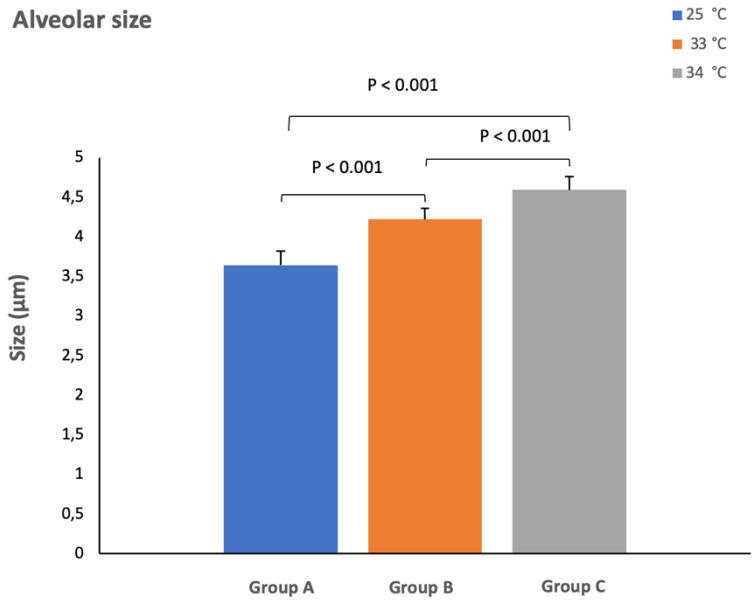


Figure 16: A graph displaying the mean Alveolar size of each group. The mean alveolar diameter is compared between group A (25 °C) and groups B and C (33 °C and 34 °C, respectively). The size of the alveoli was significantly different between all groups (p < 0.001).

With respect to the mean septal thickness, there was a significant difference between the 3 groups. A one way ANOVA was conducted to check this, resulting in P < 0.001 (table 2). Dunnett's post hoc test showed that the mean septal thickness was statistically thinner in group A (25 °C) (mean = 1.10µm ±0.34) compared to group B (33 °C) (mean = 1.82µm ±0.13) and C (34 °C) (mean = 2.35µm ±0.15) (Fig. 17). Similarly, the LSD post hoc test showed that the mean septal thickness in group B (33 °C) was significantly thinner than in group C (34 °C) (Fig. 17).

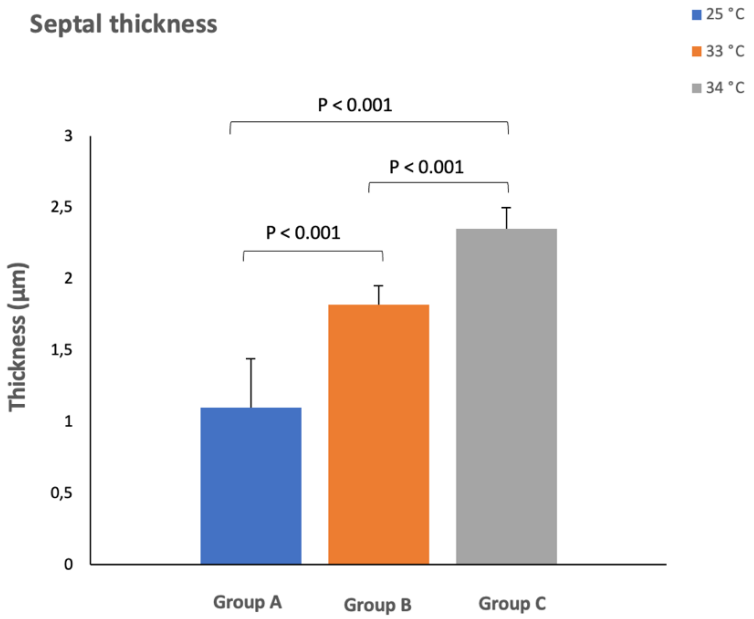


Figure 17: A graph displaying the mean thickness of the interalveolar septa. The mean septal thickness is compared between group A (25 °C) and groups B and C (33 °C and 34 °C, respectively). All three groups exhibited statistically significant mean differences in septal thickness (p < 0.001).

Table 2: The morphometric values of alveolar size and septal thickness in the three groups. The results are shown in mean ± SD. There was a significant statistical difference between the three (3) groups.

	Group A (25 °C)	**Group B (33 °C)**	**Group C (34 °C)**	**One-way Anova**
Alveolar size	3.64 µm ± 0.18	4.22 µm ± 0.14	4.59 µm ± 0.17	**P < 0.001** F = 135.095
Septal thickness	1.10 µm ± 0.34	1.82 µm ± 0.13	2.35 µm ± 0.15	**P <0.001** F= 126.169

3.4. Immunofluorescence Microscopy Analyses

Lung parenchyma

In the micrographs of the immunofluorescence labelled sections of the lung parenchyma, the anti-α-SMA is expressed to a higher degree in groups B (33 °C) and C (34 °C), in comparison to group A (25 °C) (Fig. 18. A, D, G). The micrographs of sections labelled with anti-COL2, at a low magnification, showed no apparent difference between group A (25 °C) (Fig. 18 B) and group B (33 °C) (Fig. 18 E). Group C (34 °C) exhibited a high expression of anti-COL2 relative to the other groups (Fig. 18 H). For micrographs where anti-α-SMA, anti-COL2 and DAPI overlayed, DAPI appears to have low expression in group B (33 °C) (Fig. 18 F) compared to group A (25 °C) (Fig. 18 C) and group C (34 °C) (Fig. 18 I).

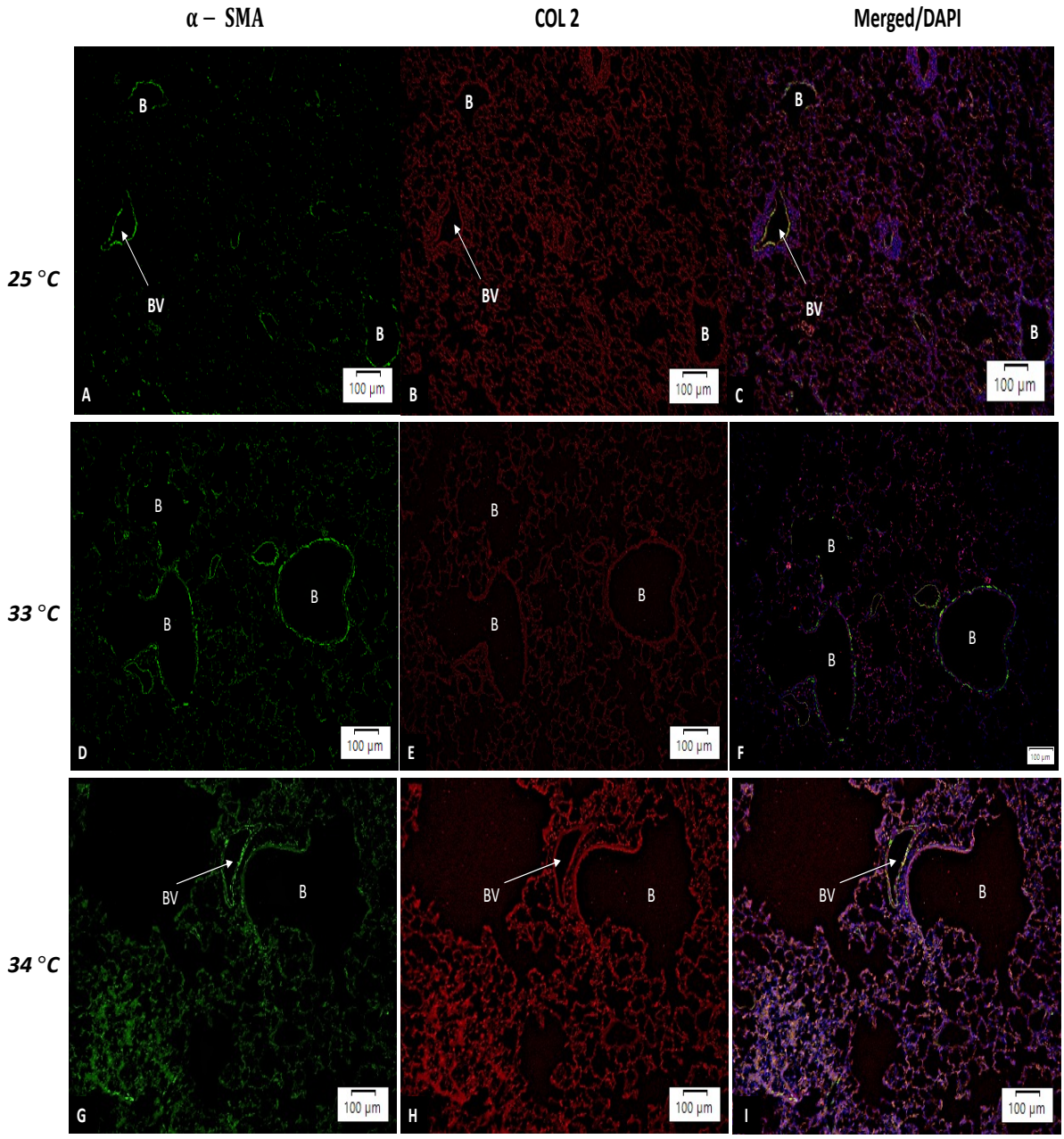


Figure 18: Micrographs of the immunolabelled sections of the lung parenchyma of the control and treatment groups. The left plates represent the anti-α-SMA antibody (1:200). The Middle plates represent the anti-COL2 antibody (1:500) and the right plates represent the merged micrographs with DAPI (1:8000). Note the high expression of anti-α-SMA in micrographs labelled 33 °C and 34 °C, respectively in comparison to 25 °C. Additionally, there was high expression of anti-COL2 in micrographs labelled 34 °C in comparison to 25 °C and 33 °C. There was higher expression of DAPI in micrographs labelled 25 °C and 34 °C compared to 33 °C.

B=Bronchioles; BV=Blood vessel; Scale bar = 100 µm

Bronchioles

In the micrographs of the immunofluorescence labelled sections of the bronchioles. Although anti-α-SMA expression was evident around the bronchioles in group A (25 °C) (Fig. 19 B), and groups B (33 °C) and C (34 °C) (Fig. 20 B, and Fig. 21 B, respectively), it was highly expressed in group C (34 °C). With respect to anti-COL2 expression, it was notable in all three groups (Fig. 19 C, 20 C, 21 C). However, group C (34 °C) exhibited higher expression of anti-COL2 around the bronchioles (Fig. 21 C) compared to other groups. In group A (25 °C), there was high DAPI expression in the epithelial bronchiole (Fig. 19 D) compared to group B (33 °C) (Fig. 20 D). Similarly, there was a higher DAPI expression around the bronchioles of group C (34 °C) (Fig. 21 D). This was especially evident around the BALT (Fig. 21 D).

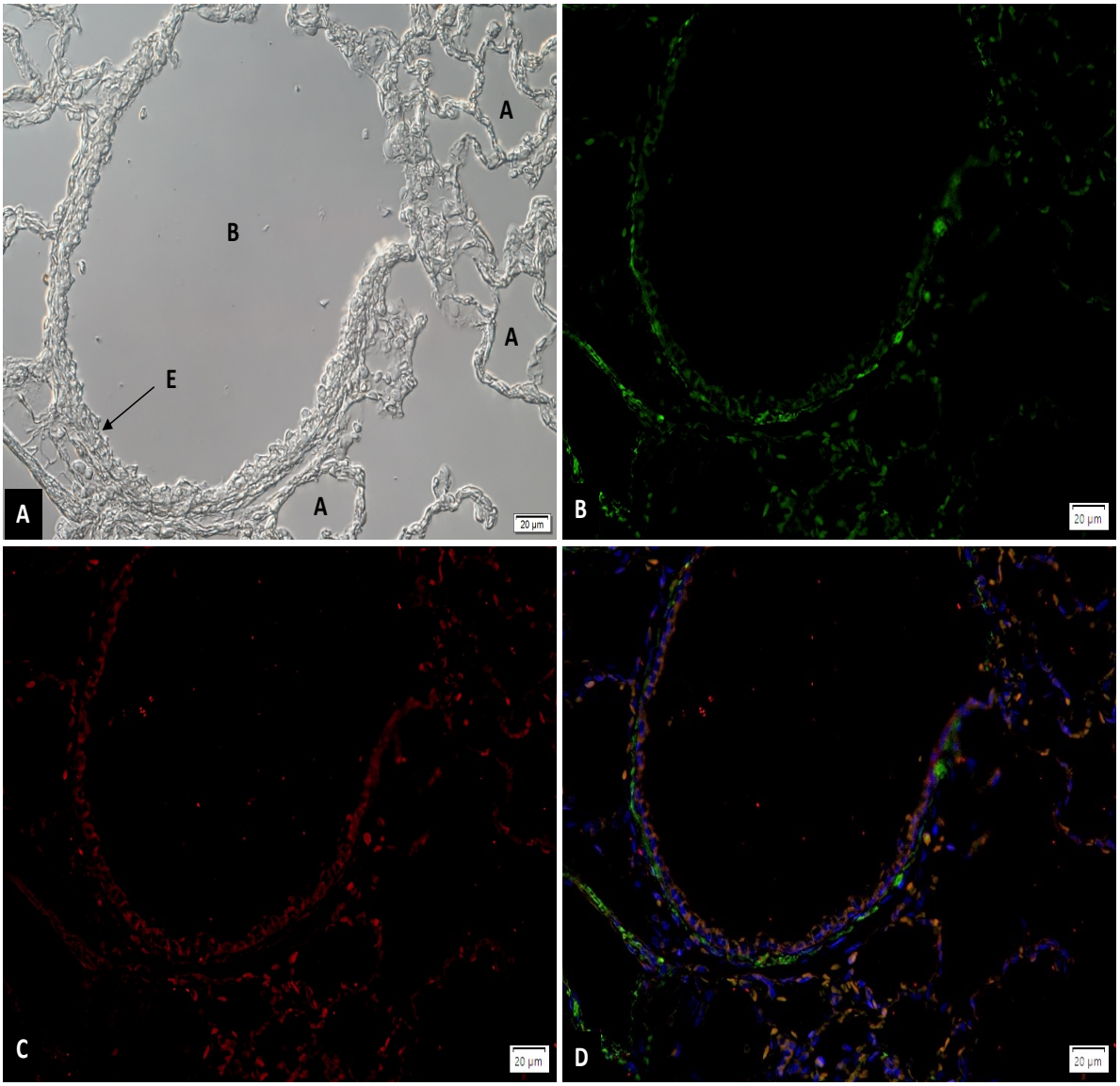


Figure 19: Micrographs of the immunolabelled sections displaying the bronchiole of group A (25 °C). (A) is a bright field micrograph representing the immunolabeled bronchioles. (B-D) note the triple labelling immunofluorescence micrographs showing anti-α-SMA, anti-COL2 and DAPI. The expression of anti-α-SMA relative to anti-COL2 is more notable in the bronchiole. In the merged/DAPI micrograph, the cells of the epithelium showed high DAPI expression.

A=Alveolus; B=Bronchiole; E=Epithelium;

Scale bar = 20 µm

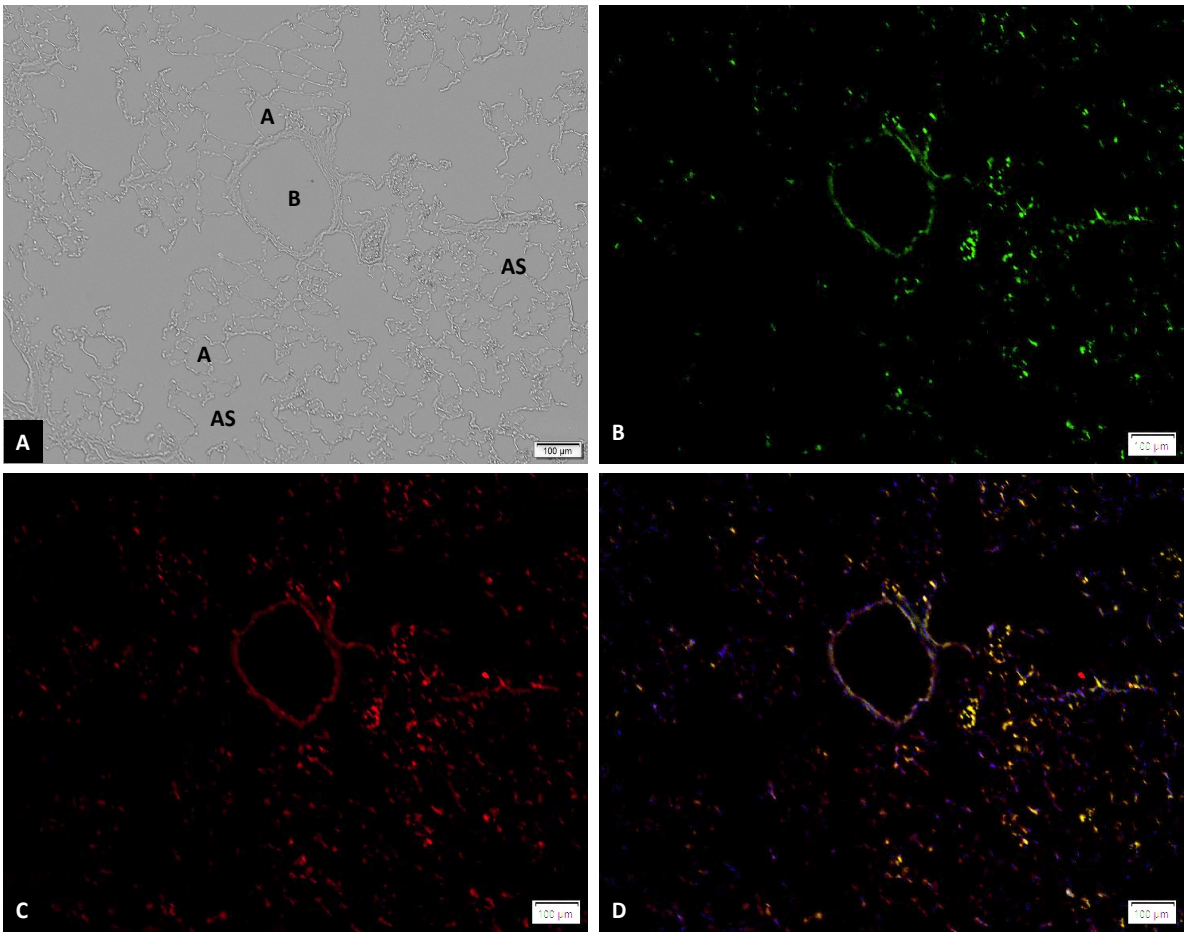


Figure 20: Micrographs of the immunolabelled sections displaying the bronchiole of group B (33 °C). (A) is a bright field micrograph representing the immunolabeled bronchioles. (B-D) note the triple labelling immunofluorescence micrographs showing anti-α-SMA, anti-COL2 and DAPI. The high expression of anti- α-SMA and anti-COL2 are notable in the bronchiole.

A=Alveoli; AS=Alveolar sac; B=Bronchiole;

Scale bar = 100 µm

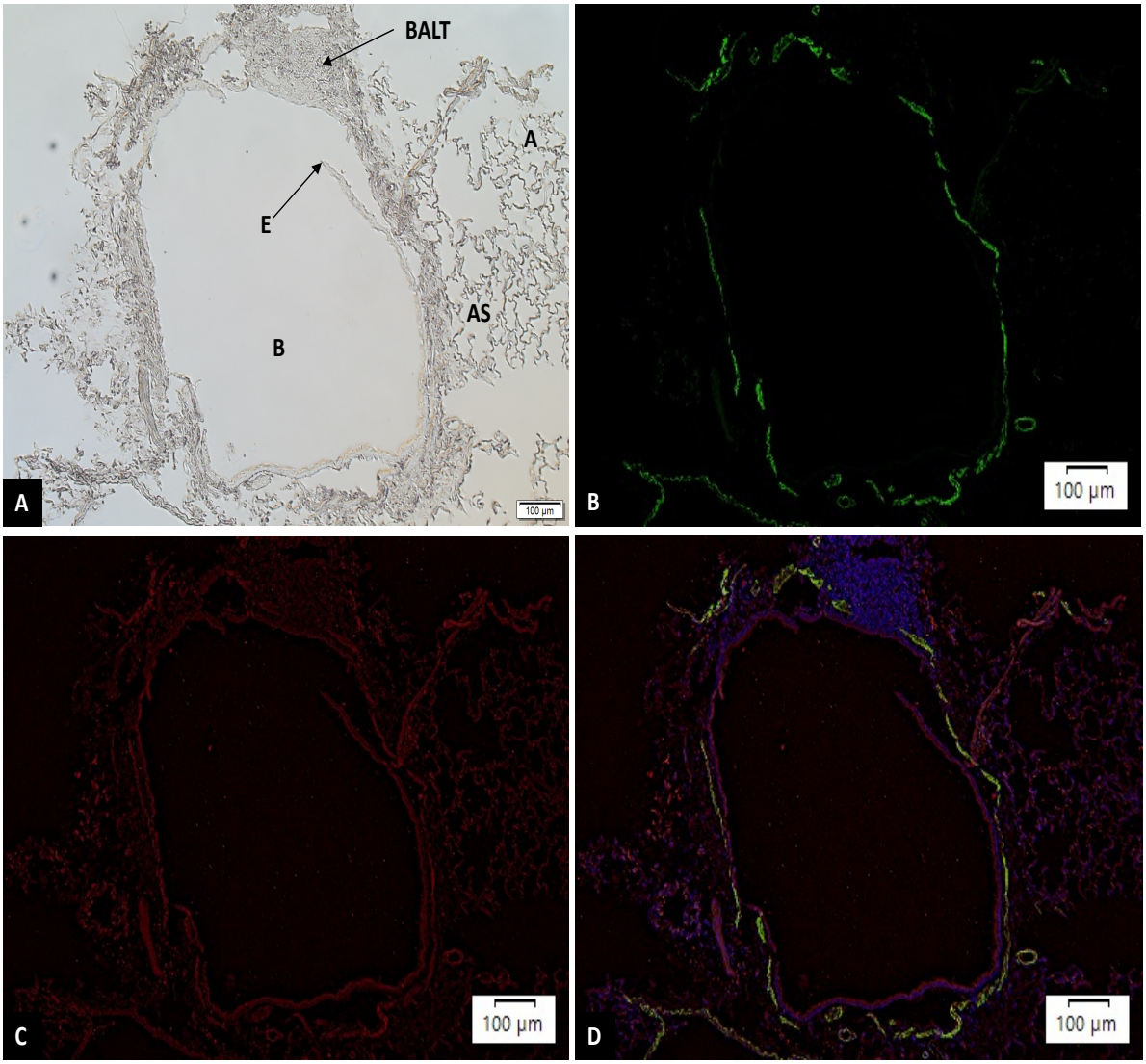


Figure 21: Micrographs of the immunolabelled sections displaying the bronchiole of treatment group C (34 °C). (A) is a bright field micrograph representing the immunolabeled bronchiole. (B-D) note the triple labelling immunofluorescence micrographs showing anti-α-SMA, anti-COL2 and DAPI. The expression of anti-α-SMA relative to anti-COL2 is more notable in the bronchiole. (D) there was high DAPI expression around the bronchiole and BALT.

A=Alveolus; AS=Alveolar sac; B=Bronchiole; BALT=Bronchus associated lymphoid tissue;

Scale bar = 100 µm

Blood vessels

In the micrographs of the immunofluorescence labelled sections of the blood vessels, the anti-α-SMA expression in group A (25 °C) (Fig. 22 B) appeared to be low relative to groups B (33 °C) and C (34 °C) (Fig. 23 B and Fig. 24 A, respectively). Interestingly, anti-α-SMA expression appeared to be more in group C (34 °C) compared to group B (33 °C) (Fig. 24 A). Even the anti-COL2 expression in group A (25 °C) (Fig. 22 C) was low compared to groups B (33 °C) and C (34 °C) (Fig. 23 C and 24 B). It was observed to be higher in group C (34 °C). With respect to DAPI expression, it was observed to be lower in group A (25 °C) (Fig. 22 D) compared to groups B (33 °C) and C (34 °C) (Fig. 23 D and Fig. 24 C, respectively). The DAPI expression appeared to be higher around the cells surrounding the blood vessels of group C (34 °C) (Fig. 24 C).

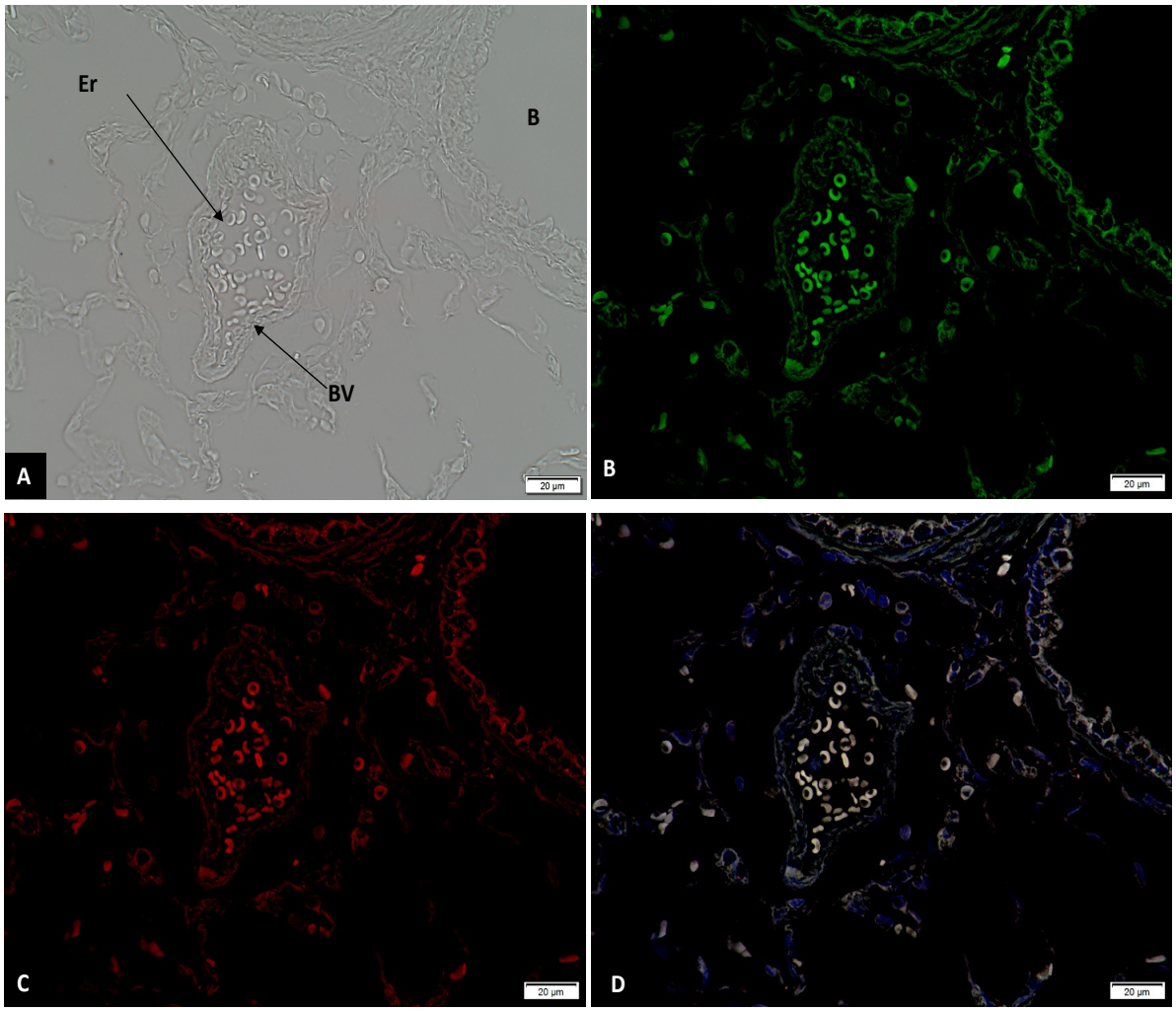


Figure 22: Micrographs of immunolabelled sections displaying the blood vessel of group A (25 °C). (A) is a bright field micrograph representing the immunolabeled blood vessel. (B-D) note the triple labelling immunofluorescence micrographs showing anti-α-SMA, anti-COL2 and DAPI. (B-C) there was low expression of anti-α-SMA and anti-COL2. (D) showed low DAPI expression in the cells of the nearby bronchiole.

B=Bronchiole; BV=Blood vessel; Er=Erythrocytes;

Scale bar = 20 µm

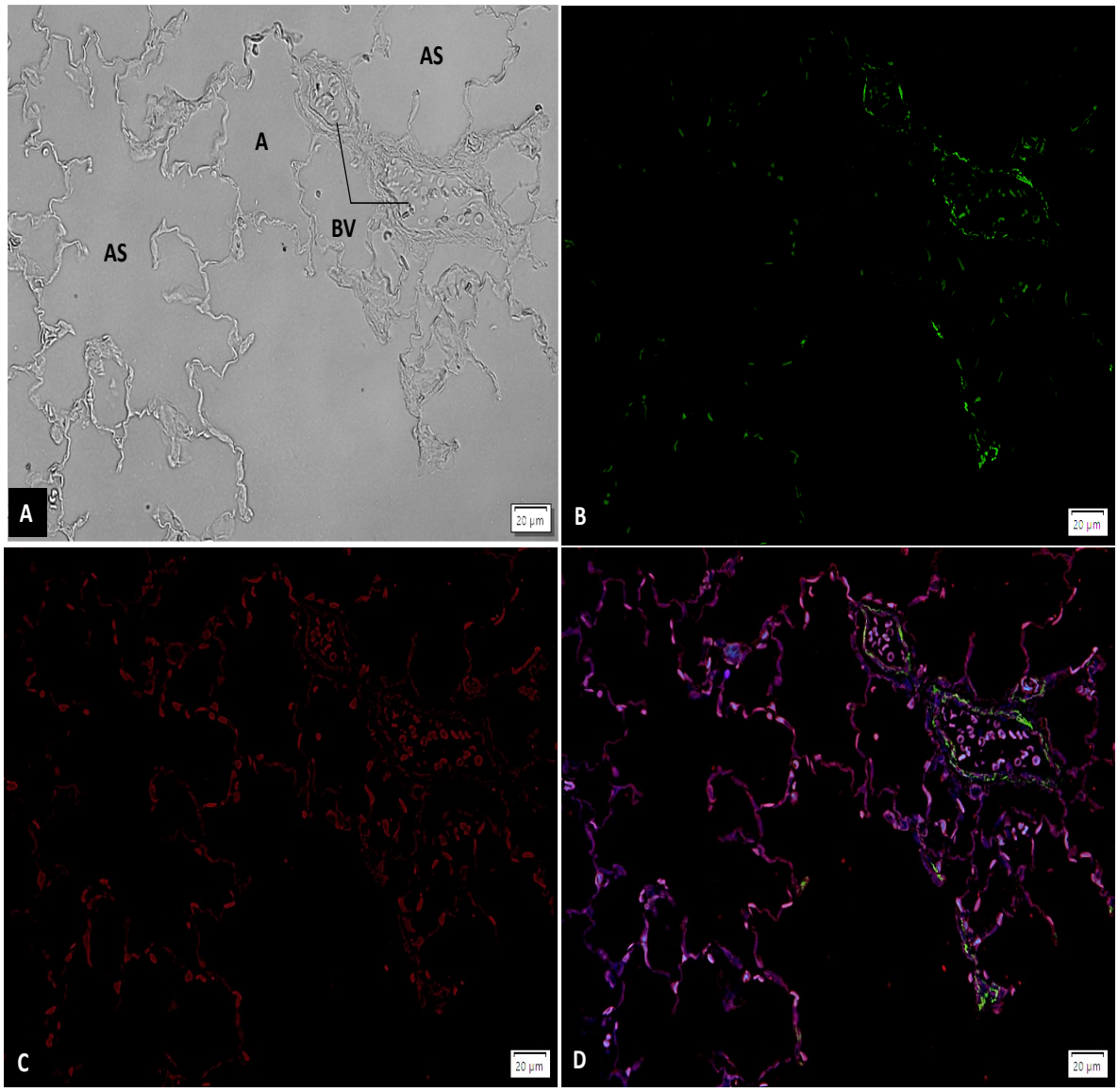


Figure 23: Micrographs of the immunolabelled sections displaying blood vessels of group B (33 °C). (A) is a bright field micrograph representing the immunolabeled blood vessel. (B-D) note the triple labelling immunofluorescence micrographs showing anti- α-SMA, anti-COL2 and DAPI. There was a high expression of anti-α-SMA and anti-COL2. (D) showed high expression of anti-α-SMA and DAPI.

A=Alveolus; AS=Alveolar sac; BV=Blood vessel;

Scale bar = 20 µm

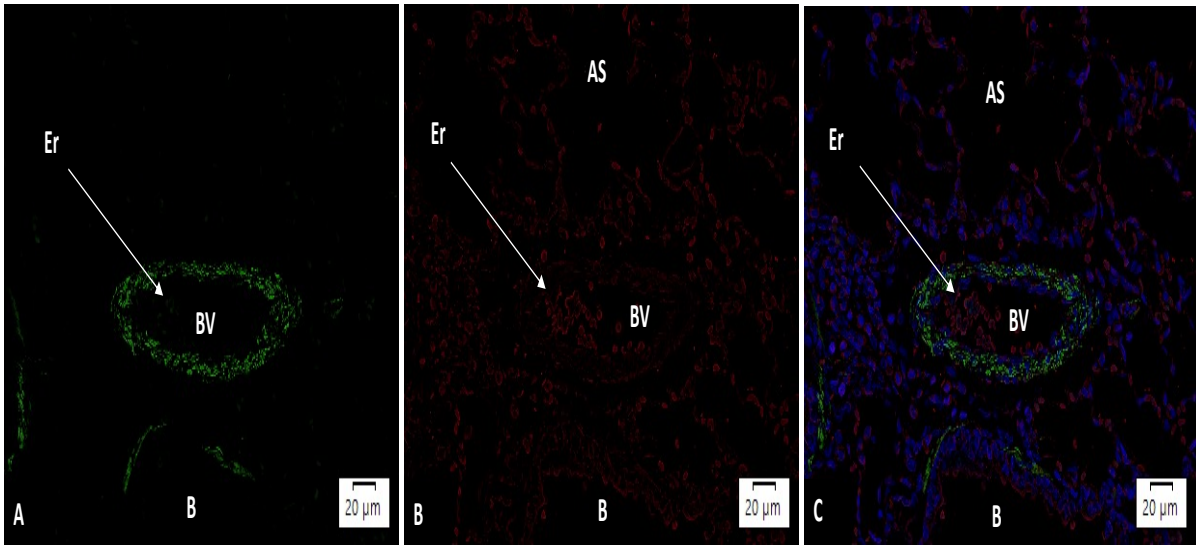


Figure 24: Micrographs of the immunolabelled sections displaying blood vessels of group C (34 °C). (A-C) note the triple labelling immunofluorescence micrographs showing anti-α-SMA, anti-COL2 and DAPI. (B-C) there was a high expression of anti-α-SMA and anti-COL2. (C) the anti- α-SMA high expression is exhibited. The cells surrounding the blood vessels exhibited high expression of DAPI.

AS= Alveolar sac; B=Bronchiole; BV=Blood vessel; Er=Erythrocytes;

Scale bar = 20 µm

4. Discussion

This study utilised histological and immunofluorescence techniques to investigate the morphological and functional changes occurring in the lungs of Sprague Dawley rats following four weeks of prolonged heat exposure. The rats were subjected to varying temperatures: Group A (25 °C), Group B (33 °C), and Group C (34 °C). It was observed that severe changes in lung morphology occur when the temperature goes above their thermoneutral zone (30-32 °C). These changes include loss of epithelial integrity, blood vessel rupture, and an increase in alveolar and bronchiole size. These changes vary relative to the different temperature levels to which each group was exposed. These new environmental temperatures compromise the respiratory function of the lungs and elicit several defence mechanisms. Some of these mechanisms are inflammation, collagen deposition, immune responses, and excess secretion of surfactant by type II alveolar cells.

These mechanisms maintained lung homeostasis, repaired cells, and showed animal acclimation to new temperatures. Correlative to this, Randall (2010) stated that the respiratory passage is vulnerable to disease, making adaptive immune responses crucial for the adaptation and survival of animals. However, prolonged maintenance of these responses can compromise lung function and hinder efficient gas exchange (Chen *et al.*, 2018). This could lead to irreversible and detrimental pulmonary diseases such as pulmonary alveolar proteinosis (PAP), lung emphysema, pulmonary oedema, and chronic obstructive pulmonary diseases.

This study selected 25 °C as the control temperature as it lies within the recommended standard reference ambient temperature of Sprague Dawley rats. As a result, it was predicted that no deviations would occur to their normal lung morphology and function within this temperature range.

The lung structure of this group displayed the homogeneous and normal structure of a healthy individual. It consisted of numerous alveoli and thin IAS. This ensures a large respiratory surface area to volume ratio (SA:V) for efficient gaseous exchange (Reddy, 2013). Thin IAS walls decrease the BGB thickness to improve the permeability of oxygen and carbon dioxide that are active in respiration (Maina & West, 2005)**.** Additionally, this group displayed a regular amount and distribution of elastic fibres around the blood vessels that became more prominent in group B (33 °C) and C (34 °C), as the heat intensity increased. These results suggest that prolonged exposure to 25 °C does not affect the lung structure. Therefore, the conservation of normal lung parenchyma in group A (25 °C) infers that efficient gas exchange took place.

The light micrographs of group B (33 °C) revealed larger blood vessels with smooth muscle hypertrophy, which is indicative of an adaptive response. Smooth muscle hypertrophy was confirmed by immunofluorescence, which revealed higher anti-α-SMA expression around the blood vessels, resulting in an amplified vasodilation response. Vasodilation is usually the first response from heat stress because it increases blood flow, which helps with heat dissipation and promotes a cooling process through sweating and convection (Ramanlal & Gupta, 2023). Finally, this indicated that vascular remodelling occurred, which helped with increased heat tolerance and circulation in this group.

Moreover, as mentioned above, in groups B (33 °C) and C (34 °C) the elastic fibres around blood vessels were more prominent than those observed in group A (25 °C). These findings correlate with the study by Annoni *et al.,* (2012) that reported prominent elastic fibres around the blood vessels with an increased temperature. Thus, it can be reasoned that the morphological changes observed in this study may be a result of functional adaptive mechanisms following heat exposure. Prominent elastic fibres enable the blood vessels to expand and recoil to maintain optimal blood flow (Annoni *et al.,* 2012; Lannoy *et al.,* 2014). This is important for optimal respiration to maintain a constant change in lung volume (Edwards & Annamaraju, 2023). As such, the findings of this study correspond with the findings of Santos *et al.,* (2002) and Voelkol & Cool (2003) about pulmonary vascular remodelling in response to heat stress. Consequently, the vascular remodelling that occurred in this study indicated that group B (33 °C) acclimatised to the heat exposure.

It is known that 95% of collagen 2 is found in the airway cartilage (Liu *et al.,* 2021). Interestingly, in this study, collagen 2 was notable in the lung parenchyma as demonstrated by the immunofluorescence micrographs. This study also found increased collagen deposition around the alveoli, bronchioles, and blood vessels in groups B (33 °C) and C (34 °C). Collagen is the major component of the extracellular matrix (ECM) which is deposited during oxidative stress and is responsible for wound healing (Matthew-Steiner *et al.,* 2021; Rodrigues *et al*., 2019). Wound healing occurs in several phases that include inflammation wherein the secretion of cytokines activates the formation of a fibrous clot at the site of injury (Matthew-Steiner *et al.,* 2021; Wells, 2022; Rodrigues *et al*., 2019). As such, the presence of collagen in the lungs of groups B (33 °C) and C (34 °C) indicates that injury occurred due to the increased heat intensity and that the tissue repairing process occurred.

It is important to note that the collagen deposition around the lungs of group C (34 °C) was significantly more excessive than in group B (33 °C). This shows the extent of damage that occurred due to the 1 °C temperature difference. Previous studies have linked excessive collagen deposition to a chronic lung disease called pulmonary fibrosis resulting in altered lung morphology (Wells, 2022; Biasin *et al*., 2017). This will result in a reduced efficiency of gaseous exchange as the amount of collagen formation, which is beyond what is needed to maintain the integrity of the damaged tissue (Wells, 2022; Matthew-Steiner *et al.,* 2021). The individuals in group C (34 °C), were unable to acclimate due to extensive tissue damage and collagen deposition. This prevented effective gaseous exchange and vascular remodelling alone was not sufficient for acclimation.

Groups B (33 °C) and C (34 °C) also displayed accumulation of BALT which is part of bronchopulmonary adaptive immune responses, triggered by chronic pulmonary inflammation or exposure to pathogens (Randall, 2010; Parlak, 2021; Sminia *et al.,* 1989). These responses are called induced BALT or iBALT (Randall, 2010; Parlak, 2021; Tschernig & Pabst, 2000). BALT works by clearing pathogens and reducing inflammation to conserve optimal lung morphology and function (Parlak, 2021). This response was absent in group A (25 °C). However, the presence of BALT in groups B (33 °C) and C (34 °C) may have been a result of pulmonary inflammation due to heat exposure. Nevertheless, this inflammatory response shortly subsided, as evidenced by the absence of macrophages and leukocytes in the alveoli space in group B (33 °C). Consequently, the level of BALT present in group B (33 °C) was significantly lower than in group C (34 °C). This implies that an adequate number of alveoli was maintained for sufficient gaseous exchange. The conservation of optimal respiratory equilibrium indicates that group B (33 °C) acclimated. This finding is complimentary with

studies by Wiley *et al*. (2009) and Randall (2010) which found that the presence of BALT leads to rapid immune responses and increased survival rates of the study animals.

Contrary to this, group C (34 °C) had visible macrophages and leukocytes, indicating that the inflammatory response persisted with excessive production of BALT. The increased amount of BALT and alveolar size resulted to a reduced SA:V, thereby affecting the rate of gaseous exchange. These findings correlate with a study by Parlak (2021) which found that the intensity and duration of heat exposure influence the amount of BALT that will be found in bronchioles. Randall (2010) also reported that when BALT levels are elevated, it can remain in the lungs for months. This will restrict normal alveolar size and function, preventing efficient gaseous exchange.

Group B (33 °C), further displayed, loss of epithelial integrity, irregular alveolar structure, thick IAS, and fewer alveoli compared to group A (25 °C). Fewer and slightly expanded alveoli suggested a slightly decreased SA:V and reduced sufficient gaseous exchange compared to group A (25 °C). These findings correlate with a study by Jin *et al*., (2011) which observed alveolar expansion and reduction in epithelial integrity in the bronchioles as heat temperature increases. The reduction in epithelial integrity may be caused by impaired mitochondrial function or inhalation of hot air into the airways (Marder, 1983). The epithelia in the lungs serve numerous functions, including the production of pulmonary surfactant, protection from harmful environmental conditions, detecting stimuli, and triggering defence mechanisms to counteract damage or injury (Waters *et al.,* 2012; Barnes *et al*., 2003). The absence of these benefits therefore increases the risk of lung damage (Barnes *et al.,* 2003). However, group B (33 °C) had minimal loss of epithelial integrity compared to group C (34 °C), where it completely detached from the bronchiole. Therefore, morphological changes observed in

group B (33 °C) indicated that the rats were under heat stress and showed adaptive changes within the lung tissue to ensure optimal gaseous exchange.

Although group C (34 °C) exhibited structural changes as those in group B (33 °C), this group had severe damage to the lung tissue. The difference in the structural changes also highlights the drastic changes that can occur due to a 1 °C temperature difference. In group C (34 °C), pulmonary oedema, formation of perivascular fluid cuffs, and PAP were observed.

In this study, pulmonary oedema may have been caused by heat-related oxidative stress. This stress could have impacted the integrity of the BGB, leading to increased permeability of the cellular membrane and subsequent leakage of fluid into the surrounding tissues.

The formation of perivascular fluid cuffs around the extra alveolar blood vessels was indicative of an inflammatory response. Normally, these cuffs help maintain lung balance by preventing fluid from building up in the alveolar space and instead directing it to the connective tissue space (Lowe *et al*., 2010). However, in this study, fluid accumulation in alveolar space occurred despite the presence of cuffs. Instead, this reduced the SA:V, which subsequently decreased pulmonary compliance and impaired the gas exchange (Lowe *et al*., 2010)

On the other hand, the accumulation of surfactant was confirmed by a positive PAS stain. However, the cause of PAP is not clear. This might be attributed to the failure of alveolar macrophages and type II pneumocytes to clear the excessive surfactant (Borie *et al.*, 2011; Zhao *et al.,* 2010).

The expansion in the size of alveoli as observed in group C (34 °C) is also a characteristic of hyperinflation that occurs due to excessive heat damage on alveoli that surpasses the threshold of an acclimatory response (Jelic, 2018). The hyperinflation of alveoli is referred to

as lung emphysema which is a form of chronic obstructive pulmonary disease (COPD) (Jelic, 2018). It becomes apparent that exposure to a temperature of 34 °C is detrimental to the respiratory function of the lung due to the severe damage that occurred. This inhibits heat acclimation as a possible response to inadequate gaseous exchange occurred.

5. Conclusion

In conclusion, exposing the lung to different temperatures within the same period results in varying degrees of structural and functional changes to the lung. These changes include loss of epithelial integrity of the bronchioles and increase in alveolar and bronchial size. Group A (25 °C) showed no structural abnormalities. In group B (33 °C), structural changes were observed but they were not as severe as those in group C (34 °C). These changes allowed the restoration of optimal lung function and heat acclimation through immune responses such as BALT accumulation and vascular remodelling.

Group C (34 °C) sustained severe immune responses that caused major morphological changes, thus inhibiting respiratory function, and preventing acclimatisation due to hindered gaseous exchange. This revealed that immune responses and vascular remodelling may not be sufficient to maintain optimal respiratory function, thus exposing the rats to pulmonary diseases that are detrimental to their survival. This further highlights the threat global warming poses on the survival of endotherms even in the presence of adaptive metabolic and physiological responses.

5.1. Recommendations

This constitutes the emergence of immediate interventions against the rise of global temperatures. To combat this, awareness needs to continue being articulated globally, including the enforcement of green initiatives as national laws and therapeutic interventions to protect and conserve species. Furthermore, it is imperative to conduct future studies that involve subjecting the study animals to higher temperatures for prolonged periods of time.

This would help to determine if their offspring would display phenotypic changes that would aid them in adapting to the environmental changes.

5.2. Study Limitations

The study's findings are limited by the absence of acute heat stress exposure, which could have provided a more comprehensive understanding of the lungs' responses across different time frames. A larger sample size would have enhanced the statistical power to draw more robust conclusions. Secondly, the use of intratracheal instillation for fixative administrations may have introduced potential alterations in lung architecture, potentially influencing the alveolar structure. Therefore, this method can be considered a potential source of artifacts in the interpretation of the study results.

6. Reference List

1. Abbass, K., Qasim, M. Z., Song, H., Murshed, M., Mahmood, H., & Younis, I. (2022). A review of the global climate change impacts, adaptation, and sustainable mitigation measures. In *Environmental Science and Pollution Research*, *29(28),* 42539–42559. https://doi.org/10.1007/s11356-022-19718-6

2. Ahmed, F., Ali, I., Kousar, S., & Ahmed, S. (2022). The environmental impact of industrialization and foreign direct investment: empirical evidence from Asia-Pacific region. *Environmental Science and Pollution Research*, *29(20),* 29778–29792. https://doi.org/10.1007/s11356-021-17560-w

3. Anderson, G. and Bell, M. (2011). Heat Waves in the United States: Mortality Risk during Heat Waves and Effect Modification by Heat Wave Characteristics in 43 U.S. Communities. *Environmental Health Perspectives*, *119(2),* 210-218. https://doi.org/10.1289/ehp.1002313

4. Anderson, G., and Bancroft, J. (2002). Tissue processing and microtomy. In: Theory and practice of histological techniques, 5th edition: 85 - 99. Bancroft, J. D., and Gamble, M. (Eds). Churchill Livingstone, London.

5. Annoni, R., Lançaş, T., Tanigawa, R. Y., Matsushita, M. D. M., Fernezlian, S. D. M., Bruno, A., Da Silva, L. F. F., Roughley, P. J., Battaglia, S., Dolhnikoff, M., Hiemstra, P. S., Sterk, P. J., Rabe, K. F., & Mauad, T. (2012). Extracellular matrix composition in COPD. *European Respiratory Journal*, *40*(6), 1362–1373. https://doi.org/10.1183/09031936.00192611

6. Barnes, P.J., Shapiro, S.D. & Pauwels, R.A. (2003). Chronic obstructive pulmonary disease: molecular and cellular mechanisms. *European Respiratory Journal*, *22*(4*),* 672-688. https://doi.org/10.1183/09031936.03.00040703

7. Biasin, V., Wygrecka, M., Marsh, L. M., Becker-Pauly, C., Brcic, L., Ghanim, B., Klepetko, W., Olschewski, A., & Kwapiszewska, G. (2017). Meprin β contributes to collagen deposition in lung fibrosis. *Scientific Reports*, *7*(1), 39969. https://doi.org/10.1038/srep39969

8. Bisgaard, H., O'Callaghan, C. & Smaldone, G. (2002). Drug delivery to the lung. *New York: M. Dekker, 1 (1),* 536. https://doi.org/10.1201/b14022

9. Borie, R., Danel, C., Debray, M. P., Taille, C., Dombret, M. C., Aubier, M., Epaud, R., & Crestani, B. (2011). Pulmonary alveolar proteinosis. In *European Respiratory Review*, *20(120),* 98–107. https://doi.org/10.1183/09059180.00001311

10. Bouchama, A., Aziz, M. A., Mahri, S. Al, Gabere, M. N., Dlamy, M. Al, Mohammad, S., Abbad, M. Al, & Hussein, M. (2017). A Model of Exposure to Extreme Environmental Heat Uncovers the Human Transcriptome to Heat Stress. *Scientific Reports*, *7(1),* 9429. https://doi.org/10.1038/s41598-017-09819-5

11. Boyles, J. G., Seebacher, F., Smit, B., & McKechnie, A. E. (2011). Adaptive thermoregulation in endotherms may alter responses to climate change. In *Integrative and Comparative Biology*, *51(5),* 676–690. https://doi.org/10.1093/icb/icr053

12. Brandt, J.P., & Mandiga, P. (2020). Histology, Alveolar Cells. *StatPearls [Internet].* StatPearls Publishing. Available: https://www.ncbi.nlm.nih.gov/books/NBK557542/

13. Brimicombe, C., Di Napoli, C., Cornforth, R., Pappenberger, F., Petty, C., & Cloke, H. L. (2021). Borderless Heat Hazards With Bordered Impacts. *Earth's Future*, *9*(9), 2064. https://doi.org/10.1029/2021EF002064

14. Brooke Anderson, G., & Bell, M. L. (2011). Heat waves in the United States: Mortality risk during heat waves and effect modification by heat wave characteristics in 43 U.S. communities. *Environmental Health Perspectives*, *119*(2), 210–218. https://doi.org/10.1289/ehp.1002313

15. Brower, M., Grace, M., Kotz, C. M., & Koya, V. (2015). Comparative analysis of growth characteristics of Sprague Dawley rats obtained from different sources. *Laboratory Animal Research*, *31*(4), 166–173. https://doi.org/10.5625/lar.2015.31.4.166

16. Bryda, E.C (2013). The Mighty Mouse: The Impact of Rodents on Advances in Biomedical Research. *Missouri State Medical Association,* 110(3), 207–211.

17. Chakraborty, S., Pattanayak, A., Mandal, S., Das, M., & Roychowdhury, R. (2014). Crop Improvement in the Era of Climate Change. *IK International Publish, 1,* 510.

18. Chan, J. (2014). The Wonderful Colors of the Hematoxylin–Eosin Stain in Diagnostic Surgical Pathology. *International Journal of Surgical Pathology*, 22(1), 12-32.

19. Chen, L., Deng, H., Cui, H., Fang, J., Zuo, Z., Deng, J., Li, Y., Wang, X., & Zhao, L. (2018). Inflammatory responses and inflammation-associated diseases in organs. *Oncotarget*, *9(6),* 7204.

20. Cheshire, W. P. (2016). Thermoregulatory disorders and illness related to heat and cold stress. *Autonomic Neuroscience*, *196*, 91–104. https://doi.org/10.1016/J.AUTNEU.2016.01.001

21. Coates, L., Haynes, K., O'Brien, J., McAneney, J. and de Oliveira, F. (2014). Exploring 167 years of vulnerability: An examination of extreme heat events in Australia 1844–2010. *Environmental Science & Policy*, *42,* 33-44. https://doi.org/10.1016/j.envsci.2014.05.03

22. Cole, E., Donnan, K. J., Simpson, A. J., & Garrett, A. T. (2023). Short-term heat acclimation protocols for an aging population: Systematic review. *PLoS ONE*, *18*(3), e0282038. https://doi.org/10.1371/journal.pone.0282038

23. Daly, N. (2021). Extreme Heat Triggers Mass Die-offs and Stress for Wildlife in the West. National Geographic. Avaiable : https://www.nationalgeographic.com/animals/article/extreme-heat-triggers-mass-die-offs-and-stress-for-wildlife-in-the-west

24. Dubray, G., & Bezard, G. (1982). A highly sensitive periodic acid-silver stain for 1, 2-diol groups of glycoproteins and polysaccharides in polyacrylamide gels. *Analytical biochemistry*, *119*(2), 325-329. https://doi.org/10.1016/0003-2697(82)90593-0

25. Ebi, K. L., Capon, A., Berry, P., Broderick, C., de Dear, R., Havenith, G., Honda, Y., Kovats, R. S., Ma, W., Malik, A., Morris, N. B., Nybo, L., Seneviratne, S. I., Vanos, J., & Jay, O. (2021). Hot weather and heat extremes: health risks. *The Lancet,* 398(10301), 698–708. https://doi.org/10.1016/S0140-6736(21)01208-3

26. Edwards, Z., & Annamaraju, P. (2023). Physiology, Lung Compliance. *StatPearls [Internet]*. StatPearls Publishing. Available: https://www.ncbi.nlm.nih.gov/books/NBK554517/

27. Engel, K. (2023). SA's West Coast Registers Record-breaking Maximum Temperatures in August. *Daily Maverick*. 23 August. Available: https://www.dailymaverick.co.za/article/2023-08-31-sas-west-coast-registers-record-breaking-maximum-temperatures-in-august/.

28. Engelbrecht, F., Adegoke, J., Bopape, M. J., Naidoo, M., Garland, R., Thatcher, M., McGregor, J., Katzfey, J., Werner, M., Ichoku, C., & Gatebe, C. (2015). Projections of rapidly rising surface temperatures over Africa under low mitigation. *Environmental Research Letters*, *10*(8), 085004. https://doi.org/10.1088/1748-9326/10/8/085004

29. Fawcett, A., & Rose, M. (2012). Guidelines for the housing of mice in scientific institutions. *Animal Welfare Unit, NSW Department of Primary Industries, West Pennant Hills, Animal Research Review Panel, 1,* 1-143.

30. Fedyaeva, A. V., Stepanov, A. V., Lyubushkina, I. V., Pobezhimova, T. P., & Rikhvanov, E. G. (2014). Heat shock induces production of reactive oxygen species and increases inner mitochondrial membrane potential in winter wheat cells. *Biochemistry (Moscow)*, *79*(11), 1202–1210.https://doi.org/10.1134/S0006297914110078

31. Frohlich, J. (2020). Rats and Mice. *Ferrets, Rabbits, and Rodents*, 1(1), 345-367. https://doi.org/10.1016/B978-0-323-48435-0.00025-3

32. Ganeshan, K., & Chawla, A. (2017). Warming the mouse to model human diseases. *Nature Reviews Endocrinology, 13(8),* 458–465. https://doi.org/10.1038/nrendo.2017.48

33. Garvey, W., Jimenez, C. and Carpenter, B. (1991). A Modified Verhoeff Elastic-van Gieson Stain. *Journal of Histotechnology*, *14(2),* 113-115.

https://doi.org/10.4081/ehj.2016.2588

34. Gaytan, F., Morales, C., Reymundo, C., & Tena-Sempere, M. (2020). A novel RGB-trichrome staining method for routine histological analysis of musculoskeletal tissues. *Scientific Reports*, *10*(1), 16659. https://doi.org/10.1038/s41598-020-74031-x

35. Gintamo, T. T., Mengistu, H., & Kanyerere, T. (2021). GIS-based modelling of climate variability impacts on groundwater quality: Cape Flats aquifer, Cape Town, South Africa. *Groundwater for Sustainable Development*, *15,* 100663. https://doi.org/10.1016/j.gsd.2021.100663

36. Glanville, E. J., Murray, S. A., & Seebacher, F. (2012). Thermal adaptation in endotherms: Climate and phylogeny interact to determine population-level responses in a wild rat. *Functional Ecology*, *26*(2), 390–398. https://doi.org/10.1111/j.1365-2435.2011.01933.x

37. Greene, S., Kalkstein, L.S., Mills, D.M. & Samenow, J. (2011). An examination of climate change on extreme heat events and climate–mortality relationships in large US cities. *Weather, Climate, and Society*, *3*(4), 281-292. https://doi.org/10.1175/WCAS-D-11-00055.1

38. Hakim, A., & Usmani, O. S. (2014). Structure of the Lower Respiratory Tract. *Reference Module in Biomedical Sciences*. https://doi.org/10.1016/B978-0-12-801238-3.00215-4

39. Hanania, J., Vargas Suarez, L., Donev, J.(2020). Energy Education – Heat wave [Online]. Available: https://energyeducation.ca/encyclopedia/Heat_wave

40. Hankenson, F.C., Marx, J. O., Gordon, C. J., & David, J.M. (2018). Effects of Rodent Thermoregulation on Animal Models in the Research Environment. *Comparative Medicine, 68(6),* 425-438. https://doi.org/10.30802/AALAS-CM-18-000049

41. Horowitz, M. (1998). Do Cellular Heat Acclimation Responses Modulate Central Thermoregulatory Activity. *Physiology*, *13(5)*, 218-225. https://doi.org/10.1152/physiologyonline.1998.13.5.218

42. Horowitz, M. (2002). From molecular and cellular to integrative heat defense during exposure to chronic heat. *Comparative Biochemistry and Physiology Part A: Molecular & Integrative Physiology*, *131(3),* 475-483. https://doi.org/10.1016/s1095-6433(01)00500-1

43. Hugo, J. M. (2023). Heat Stress: Adaptation Measures in South African Informal Settlements. *Buildings and Cities*. 4(1), 55–73.

44. Im, K., Mareninov, S., Diaz, M. F. P., & Yong, W. H. (2019). An introduction to performing immunofluorescence staining. *Biobanking: methods and protocols*, *1897*, 299–311. https://doi.org/10.1007/978-1-4939-8935-5_26

45. Intergovernmental Panel on Climate Change. 2022. *Climate Change 2022: Impacts, Adaptation, and Vulnerability*. Available: https://www.ipcc.ch/report/ar6/wg2/chapter/summary-for-policymakers/

46. Jelic, T. M. (2018). Emphysema. *Updates in Respiratory Diseases*. Garcia, J. H. C., Ed. https://doi.org/10.5772/intechopen.83273

47. Jin, Y., Hu, Y., Han, D., & Wang, M. (2011). Chronic Heat Stress Weakened the Innate Immunity and Increased the Virulence of Highly Pathogenic Avian Influenza Virus H5N1 in Mice. *Journal of Biomedicine and Biotechnology*, *2011,* e367846. https://doi.org/10.1155/2011/367846

48. Kapwata, T., Gebreslasie, M. T., & Wright, C. Y. (2022). An analysis of past and future heatwaves based on a heat-associated mortality threshold: towards a heat health warning system. *Environmental Health: A Global Access Science Source*, *21(1),* 112. https://doi.org/10.1186/s12940-022-00921-4

49. Kazemi, A., Louis, B., Isabey, D., Nieman, G. F., Gatto, L. A., Satalin, J., Baker, S., Grotberg, J. B., & Filoche, M. (2019). Surfactant delivery in rat lungs: Comparing 3D geometrical simulation model with experimental instillation. *PLoS Computational Biology*, *15*(10), e10007408. https://doi.org/10.1371/journal.pcbi.1007408

50. Khan, Y.S. & Lynch, D.T. (2018). Histology, Lung. *StatPearls [internet]*. StatPearls Publishing. Availabe: https://www.ncbi.nlm.nih.gov/books/NBK534789/

51. Kling, M.A. (2011). A review of respiratory system anatomy, physiology, and disease in the mouse, rat, hamster, and gerbil. *Veterinary Clinics: Exotic Animal Practice*, *14*(2), 287-337. https://doi.org/10.1016/j.cvex.2011.03.007

52. Knudsen, L., & Ochs, M. (2018). The micromechanics of lung alveoli: structure and function of surfactant and tissue components. *Histochemistry and Cell Biology*, *150(6),* 661–676. https://doi.org/10.1007/s00418-018-1747-9

53. Lannoy, M., Slove, S. & Jacob, M.P. (2014). The function of elastic fibers in the arteries: beyond elasticity. *Pathologie Biologie*, *62(2),* 79-83. https://doi.org/10.1016/j.patbio.2014.02.011

54. Leiby, K., & Raredon, M., & Niklason, L. (2020). Bioengineering the Blood-gas Barrier. *Comprehensive Physiology, 10(2),* 415-452. https://doi.org/10.1002/cphy.c190026

55. Li, X., Stringer, L. C., & Dallimer, M. (2022). The Impacts of Urbanisation and Climate Change on the Urban Thermal Environment in Africa. *Climate, 10(11),* 164. https://doi.org/10.3390/cli10110164

56. Liu, L., Stephens, B., Bergman, M., May, A., & Chiang, T. (2021). Role of Collagen in Airway Mechanics. *Bioengineering, 8(1),* 13. https://doi.org/10.3390/bioengineering8010013

57. Liu, Z.-F., Li, B.-L., Tong, H.-S., Tang, Y.-Q., Xu, Q.-L., Guo, J.-Q., & Su, L. (2011). Pathological changes in the lung and brain of mice during heat stress and cooling treatment. *World Journal Emergency Medicine, 2*(1), 50-53. https://doi.org.10.5847/wjem.j.1920-8642.2011.01.009

58. Liu, Z., Sun, X., Tang, J., Tang, Y., Tong, H., Wen, Q., Liu, Y. and Su, L. (2011). Intestinal inflammation and tissue injury in response to heat stress and cooling treatment in mice. *Molecular medicine reports, 4(3),* 437-443. https://doi.org/10.3892/mmr.2011.461

59. Lowe, K., Alvarez, D. F., King, J. A., & Stevens, T. (2010). Perivascular fluid cuffs decrease lung compliance by increasing tissue resistance. *Critical care medicine, 38(6),* 1458-1466. https://doi.org/10.1097/CCM.0b013e3181de18f0

60. Luber, G., & McGeehin, M. (2008). Climate Change and Extreme Heat Events. *American Journal of Preventive Medicine, 35(5),* 429-435. https://doi.org/10.1016/j.amepre.2008.08.021

61. Lugo-Amador, N. M., Rothenhaus, T., & Moyer, P. (2004). Heat-related illness. *Emergency Medicine Clinics of North America,* 22(2), 315–327. https://doi.org/10.1016/j.emc.2004.01.004

62. Ma, W., Zeng, W., Zhou, M., Wang, L., Rutherford, S., Lin, H., Liu, T., Zhang, Y., Xiao, J., Zhang, Y., Wang, X., Gu, X., & Chu, C. (2015). The short-term effect of heat waves on mortality and its modifiers in China: An analysis from 66 communities. *Environment International*, *75*, 103–109. https://doi.org/10.1016/J.ENVINT.2014.11.004

63. Maina, J. N., & West, J. B. (2005). Thin and strong! The bioengineering dilemma in the structural and functional design of the blood-gas barrier. *Physiological reviews*, *85*(3), 811–844. https://doi.org/10.1152/physrev.00022.2004

64. Makanya, A., Anagnostopoulou, A., & Djonov, V. (2013). Development and Remodeling of the Vertebrate Blood-Gas Barrier. *BioMed Research International*, *20(13)*, 1-15. https://doi.org/10.1155/2013/101597

65. Maloyan, A., Palmon, A., & Horowitz, M. (1999). Heat acclimation increases the basal HSP72 level and alters its production dynamics during heat stress. *Am J Physiol, 276(5),* 1506-1515. https://doi.org/10.1152/ajpregu.1999.276.5.R1506

66. Marder, J. (1983). Cutaneous water evaporation - II. Survival of birds under extreme thermal stress. *Comp Biochm Physiol,* 75(3)**,** 433-439. https://doi.org/10.1016/0300-9629(83)90106-8.

67. Mason, R.J. (2006). Biology of alveolar type II cells. *Respirology*, *11*, S12-S15.

68. Matthew-Steiner, S. S., Roy, S., & Sen, C. K. (2021). Collagen in Wound Healing. *Bioengineering, 63(8),* 1-15. https://doi.org/10.3390/bioengineering8050063

69. McKechnie, A. E., & Wolf, B. O. (2019). The physiology of heat tolerance in small endotherms. *American Physiological Society, 35(5),* 302–313. https://doi.org/10.1152/physiol.00011.2019

70. Meehl, G. & Tebaldi, C. (2004). More Intense, More Frequent, and Longer Lasting Heat Waves in the 21st Century. *Science, 305(5686*), 994-997. https://doi.org/10.1126/science.1098704

71. Mentel, U., Wolanin, E., Eshov, M., & Salahodjaev, R. (2022). Industrialization and CO2 Emissions in Sub-Saharan Africa: The Mitigating Role of Renewable Electricity. *Energies*, *15*(3), 946. https://doi.org/10.3390/en15030946

72. Mercer, R. R., & Crapo, J. D. (1993). Lower respiratory tract structure of laboratory animals and humans: Dosimetry implications. *Aerosol Science and Technology*, *18*(3), 257–271. https://doi.org/10.1080/02786829308959603

73. National Centres for Environmental Information, (2021). NOAA National Centers for Environmental Information, Monthly Global Climate Report for Annual 2021, published online January 2022, retrieved on November 1, 2022, from https://www.ncei.noaa.gov/access/monitoring/monthlyreport/global/202113

74. Obernier, J. A., & Baldwin, R. L.(2006). Establishing an Appropriate Period of Acclimatization Following Transportation of Laboratory Animals. *ILAR Journal, 47(4),* 364-369. https://doi.org/10.1093/ilar.47.4.364

75. Parlak AK, T. (2021). Bronchus-Associated Lymphoid Tissue (BALT) Histology and Its Role in Various Pathologies. *Updates on Veterinary Anatomy and Physiology*, *9(9),* 366. https://doi.org/10.5772/intechopen.99366

76. Patwa, A. & Shah, A. (2015). Anatomy and physiology of respiratory system relevant to anesthesia. *Indian Journal of Anesthesia*, *59*(9), 533-541. https://doi.org/10.4103/0019-5049.165849

77. Permenter, M. G., McDyre, B. C., Ippolito, D. L., & Stallings, J. D. (2019). Alterations in tissue microRNA after heat stress in the conscious rat: Potential biomarkers of organ-specific injury. *BMC Genomics*, *20*(1), 141. https://doi.org/10.1186/s12864-019-5515-6

78. Petkova, E. P., Morita, H., & Kinney, P. L. (2014). Health Impacts of Heat in a Changing Climate: How Can Emerging Science Inform Urban Adaptation Planning?. *Current Epidemiology Reports, 1(2)*, 67-74. https://doi.org/10.1007/s40471-014-0009-1

79. Pittman, R. N. (2011). Regulation of Tissue Oxygenation. *Morgan and Claypool Life Sciences*. California: San Rafael. Available: https://www.ncbi.nlm.nih.gov/books/NBK54104/

80. Ramanlal, R., & Gupta, V. (2023). Physiology, Vasodilation. StatPearls[Internet]. *StatPearls Publishing.* Available: https://pubmed.ncbi.nlm.nih.gov/32491494/

81. Randall, T. D. (2010). Bronchus-associated lymphoid tissue (BALT): structure and function. *Advances in immunology*, 107, 187-241. https://doi.org/10.1016/S0065-2776(10)07002-1

82. Reddy, D. (2013). A Morphological and Morphometric Investigation into the Morphogenesis of the Crocodilian Lung. Doctor of Philosophy. Available at: University of the Witwatersrand.

83. Rodrigues, M., Kosaric, N., Bonham, C. A., & Gurtner, G. C. (2019). Wound Healing: A Cellular Perspective. *Physiological Reviews*. 99(1), 665-706. https://doi.org/10.1152/physrev.00067.2017.-Wound

84. SANS (2008). South African National Standards. The care and use of animals for scientific purposes, 1st edition. SABS Standards Division, Pretoria, South Africa.

85. Santos, R. M., & Bakhshoodeh, R. (2021). Climate change/global warming/climate emergency versus general climate research: comparative bibliometric trends of publications. *Heliyon*, *7*(11), e08219. https://doi.org/10.1016/j.heliyon.2021.e08219

86. Sareh, H., Tulapurkar, M., Shah, N., Singh, I. and Hasday, J. (2010). Response of mice to continuous 5-day passive hyperthermia resembles human heat acclimation. *Cell Stress and Chaperones*, 16(3), 297-307. https://doi.org/10.1007/s12192-010-0240-8

87. Schindelin, J., Arganda-Carreras, I., Frise, E., Kaynig, V., Longair, M., Pietzsch, T., Preibisch, S., Rueden, C., Saalfeld, S., Schmid, B., Tinevez, J.-Y., White, D. J., Hartenstein, V., Eliceiri, K., Tomancak, P. & Cardona, A. (2012). Fiji: an open-source platform for biological-image analysis. *Nat Methods,* 9, 676-682. https://doi.org/10.1038/nmeth.2019

88. Scholes, R., & Engelbrecht, F. (2021). Climate impacts in southern Africa during the 21 st Century. Available: https://www.globalcarbonproject.org/carbonbudget/20

89. Schwimmer, H., Gerstberger, R. & Horowitz, M. (2004). Heat acclimation affects the neuromodulatory role of AngII and nitric oxide during combined heat and hypohydration stress. *Molecular Brain Research*, *130*(1-2), 95-108. https://doi.org/10.1016/j.molbrainres.2004.07.011

90. Simandan, D. (2009). Industrialization. *International Encyclopedia of Human Geography, 5,* 419-425.

91. Sminia, T., Van der Brugge-Gmelkoorn, G.J., & Jeurissen, S. H. (1989). Structure and function of bronchus-associated lymphoid tissue (BALT). *Critical reviews in immunology*, *9(2),* 119-150.

92. Suckow, M.A., Weisbroth, S.H. & Franklin, C.L. (2005). *The laboratory rat*. Elsevier

93. Suki, B., Stamenović, D., & Hubmayr, R. (2011). Lung parenchymal mechanics. *Comprehensive Physiology*, *1*(3), 1317–1351. https://doi.org/10.1002/cphy.c100033

94. Toesland, F. (2019). Africa's Megacities a Magnet for Investors. *United Nations*. Available: https://www.un.org/africarenewal/magazine/april-2019-july-2019/africa's-megacities-magnet-investors

95. Tschernig, T., & Pabst, R. (2000). Bronchus-Associated Lymphoid Tissue (BALT) Is Not Present in the Normal Adult Lung but in Different Diseases. *Pathobiology*, 68 (1), 1–8. https://doi.org/10.1159/000028109

96. United States Environmental Protection Agency. (2023). Climate Change Impacts on Agriculture and Food Supply. Available: https://www.epa.gov/climateimpacts/climate-change-impacts-agriculture-and-food-supply

97. Voelkel, N. F., Douglas, I. S., & Nicolls, M. (2003). Angiogenesis in Chronic Lung Disease. *Chest, 131(3),* 874-879. https://doi.org/10.1378/chest.06-2453

98. Waters, C. M., Roan, E., & Navajas, D. (2012). Mechanobiology in lung epithelial cells: Measurements, perturbations, and responses. *Comprehensive Physiology*, *2(1),* 1–29. https://doi.org/10.1002/cphy.c100090

99. Wells, R. G. (2022). How Collagen Becomes 'stiff'. *Elife*, *11,* 77041. https://doi.org/10.7554/eLife.77041

100. West, J. B., & Mathieu-Costello, O. (1999). Structure, strength, failure, and remodeling of the pulmonary blood-gas barrier. *Annual review of physiology, 61(1),* 543-572. https://doi.org/10.1146/annurev.physiol.61.1.543

101. Wheeler, D. S., & Wong, H.R. (2006). Heat shock response and acute lung injury. *Free Radical Biology and Medicine, 42(1*), 1-14. https://doi.org/10.1016/j.freeradbiomed.2006.08.028

102. Whitsett, J. A., Wert, S. E., & Weaver, T. E. (2010). Alveolar surfactant homeostasis and the pathogenesis of pulmonary disease. *Annual Review of Medicine, 61,* 105–119. https://doi.org/10.1146/annurev.med.60.041807.123500

103. Wiley, J. A., Richert, L. E., Swain, S. D., Harmsen, A., Barnard, D.L., Randall, T. D., Jutila, M., Douglas, T., Broomell, C., Young, M. & Harmsen, A. (2009). Inducible bronchus-associated lymphoid tissue elicited by a protein cage nanoparticle enhances protection in mice against diverse respiratory viruses. *PloS one*, *4(9),* e7142. https://doi.org/10.1371/journal.pone.0007142

104. World Economic Forum. 2022. *Five Ways to Help Wildlife in Heatwaves*. Available: https://www.weforum.org/agenda/2022/07/wildlife-heatwaves-climate-change-animal-welfare

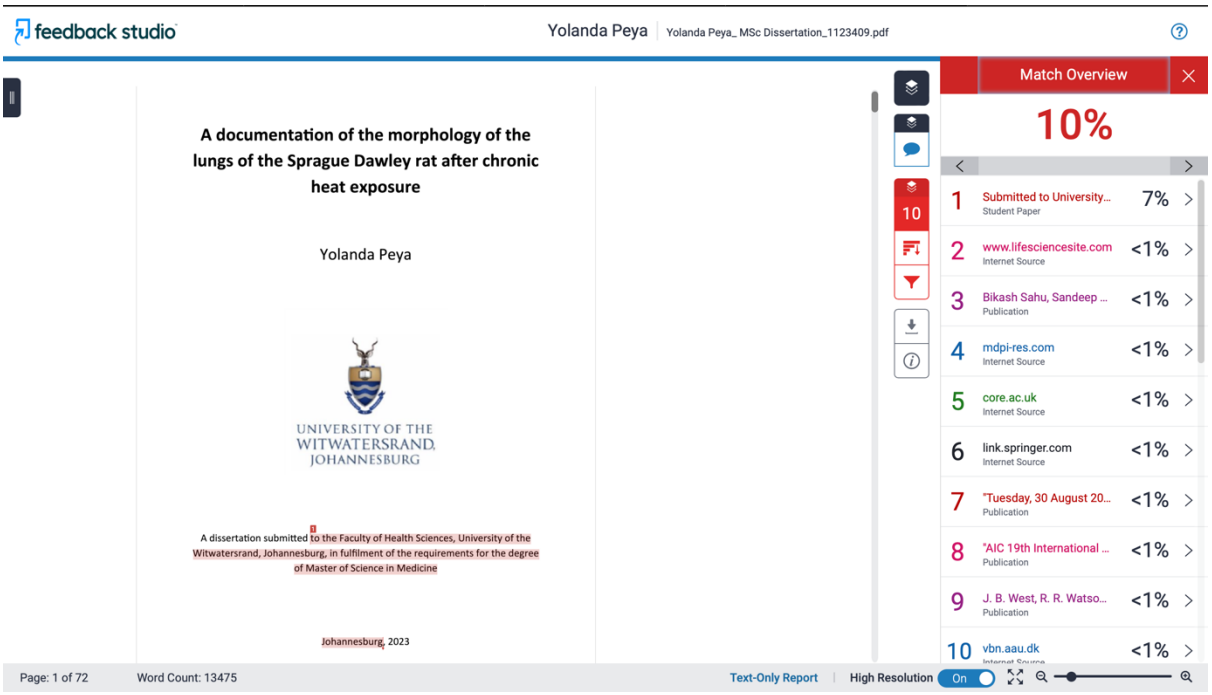
105. Xiang, J., Bi, P., Pisaniello, D. & Hansen, A. (2014). Health impacts of workplace heat exposure: an epidemiological review. *Industrial health*, *52(2),* 91-101. https://doi.org/10.2486/indhealth.2012-0145

106. Yan, Y. E., Zhao, Y. Q., Wang, H., & Fan, M. (2006). Pathophysiological factors underlying heatstroke. *Medical Hypotheses*, *67*(3), 609–617. https://doi.org/10.1016/j.mehy.2005.12.048

107. Zhao, C., Fang, X., Wang, D., Tang, F. 2010. Involvement of type II pneumocytes in the pathogenesis of chronic obstructive pulmonary disease. *Respiratory Medicine, 104(10),* 1391-1395. https://doi.org/10.1016/j.rmed.2010.06.018

7. Appendices

Appendix 1: Turnitin report



Appendix 2: Ethics waiver

ANIMAL RESEARCH ETHICS COMMITTEE
Registration number: AREC-101210-002

Date: 03/02/2023

Certificate reference: Waiver 03-02-2023-O
Category: O
Applicant: Yolanda Peya
Department: School of Anatomical Sciences (WITS)
Tel: 011 717 2713; **Email**: 1123409@students.wits.ac.za

Re: Waiver from the Animal Ethics Research Committee of the University of the Witwatersrand

This letter is to confirm that Yolanda Peya, MSc (Med) student (#1123409) under the supervision of Dr Deran Reddy (School of Anatomical Sciences), does not require full Animal Ethics Research Committee clearance to undertake the work titled **'A Morphological Study of The Respiratory System of The Sprague Dawley Rat After Chronic Heat Exposure'**.

Reason for waiver
The project is using samples already collected from a completed study that was done by Caitlin Stainbank, titled "The histology of heat stressed lungs in Sprague Dawley rats after two and four weeks of persistent heat exposure" (AREC #2019/04/19/C)

Details of the study
The project will assess the effect of chronic heat exposure on the gross morphology of the lung and extra pulmonary airways, on the histology of the lung and extrapulmonary airways by means of multiple staining techniques and on the major structural components by means of Immunofluorescence. The applicant will finally perform a histomorphometric analysis on the size of the alveoli, the thickness of Septa and major structural components.

The individual covered by the waiver are Yolanda Peya and Dr Deran Reddy (Wits).

Please contact me should you require further information.

Yours sincerely

Prof Frederic Michel
Chair: Animal Research Ethics Committee
University of the Witwatersrand

Appendix 3: Ethics approval certificate

UNIVERSITY OF THE WITWATERSRAND JOHANNESBURG

STRICTLY CONFIDENTIAL

ANIMAL RESEARCH ETHICS COMMITTEE (AREC)

CLEARANCE CERTIFICATE NO. 2019/04/19/C

APPLICANT: Ms C Stainbank

SCHOOL: Animal, Plant and Environmental Sciences
DEPARTMENT:
LOCATION:

PROJECT TITLE: The histology of heat stressed lungs in Sprague Dawley rats after two and four weeks of persistent heat exposure

Number and Species

32X 6-8 weeks, 250-300g male and female domesticus Rattus norvegicus

Approval was given for the use of animals for the project described above at an AREC meeting held on 2019/04/30. This approval remains valid until 2019/07/28.
Unreported changes to the application may invalidate the clearance given by the AREC
An annual progress report must be provided

The use of these animals is subject to AREC guidelines for the use and care of animals, is limited to the procedures described in the application form and is subject to any additional conditions listed below:

Signed: _____ (Chairperson, AREC) Date: 8/8/2019

I am satisfied that the persons listed in this application are competent to perform the procedures therein, in terms of Section 23 (1) (c) of the Veterinary and Para-Veterinary Professions Act (19 of 1982)

Signed: _____ (Registered Veterinarian) Date: 29 July 2019

cc: Supervisor: Dr D Reddy
Director: CAS

Works 2000/Iain0015/AESCCert.wps

Appendix 4: Tissue Processing

The tissue was processed using an automatic tissue processor (Shandon Citadel 1000) as follows:

1. 10% buffered formalin 4 hours
2. 70% alcohol for 1 hour
3. 95% alcohol for 2 hours
4. 95% alcohol for 1.5 hours
5. 95% alcohol for 1.5 hours
6. 100% Alcohol for 1 hour
7. 100% Alcohol for 2 hours
8. 100% Alcohol for 1 hour
9. Chloroform for 2 hours
10. Chloroform for 2 hours
11. Wax for 2 hours
12. Wax for 2 hours

Appendix 5: Haematoxylin and Eosin staining

Reagents used

- Haematoxylin 1 g
- 1000mL Distilled water 1000 mL
- 50.0 g Ammonium alum 50 g
- 0.2g Sodium iodate 0.2 g
- 1.0 g Citric acid 1 g
- 50 g Chloral hydrate 50 g

Eosin reagents used;

- Eosin Y (water soluble)
- Distilled water

Hydration

1. Dewax slides in two changes of xylene for 10 minutes
2. Immerse in two changes of 100 % ethanol for 3 minutes each
3. Immerse in 95% ethanol for 3 minutes
4. Immerse in 70% for 3 minutes
5. Wash in distilled water for 5 minutes

The staining procedure; Haematoxylin and Eosin (H&E)

1. Dewax and hydrate (following hydration steps)
2. Place slide in Haematoxylin for 10 minutes
3. Wash slides in running water for 5 minutes
4. Dip slides in 1% Acid Alcohol for 5 minutes(Optional)
5. To counterstain; place the slide in Eosin for 30s to 1 minute
6. Wash slides in running water
7. Dehydrate through 70%, 95% and 100% (10 dips or 30s)
8. Place slide in two changes of xylene for 2 minutes each
9. Coverslip and let the slides dry

Appendix 6: New pentachrome stain

Reagents used:

- 10% Formaldehyde
- 6% Nitric Acid
- 0.5% Toluidine Blue Solution
- Picrosirius staining solution
- Alcoholic Picrosirius staining solution (Optional)

Staining procedure

1. Place slides in a staining rack
2. Dewax and Hydrate slides
3. Pre-treat with 6% Nitric acid for 5 minutes and directly place the slide in Toluidine Blue solution
4. Stain with 0.5% Toluidine Blue Solution for 5 minutes.
5. Wash in running tap water until the water becomes clear
6. Stain with Picrosirius Solution for 5 minutes.
7. Wash in running tap water
8. Stain with an Alcoholic Picrosirius Solution for 5 minutes.
9. Dehydrate through an ascending series of alcohol changes; 70%, 95% and 100% (10 dips or 30s).
10. Submerge to two changes of xylene.
11. Mount slide in Entellen and coverslip

Results

Collagen in red, sulphated mucopolysaccharides in violet, muscles in orange, erythrocytes in yellow, and nuclei in green.

Appendix 7: Van Geison Stain

Reagents used:

- 3% Alcoholic Haematoxylin
- 2% Ferric Chloride, Aqueous
- Lugo's Iodine
- Van Geisons Solution
- 0.4 % Aqueous ferric chloride

Staining procedure

1. Place slides in a rack
2. Dewax and hydrate (following the steps, as seen in Mayer's H&E)
3. Stain the slides in Verhoeff at room temperature for 7 minutes or 3.5 minutes at 60 ^{o}C oven.
4. Prepare the modified Verhoeff working elastic solution (before use) using;

    - 3 parts 3% Alcoholic Haematoxylin,
    - 2 parts 2% Aqueous Ferric Chloride,
    - 3) 1 part Lugo's iodine.

5. Wash in running tap water and carefully agitate the slides for 1 minute
6. Place slides in 0.4% Aqueous Ferric Chloride for 75 seconds
7. Wash in running tap water for 5 minutes
8. Place in Van Geison solution for 1 minute
9. Dehydrate through an ascending series of alcohol changes; 70%, 95% and 100% (10 dips or 30s)
10. Place in two changes of xylene
11. Mount slides with Entellan and coverslip

Results:

Elastic fibres and nuclei in black, collagen red, and muscle fibres are yellow

Appendix 8: Red Green Blue (RGB) Trichrome Stain

Reagents used;

- 1% Alcian blue in 3% aqueous acetic acid solution (pH 2.5)
- 0.04% fast green solution
- 0.1% picrosirius red solution

Staining procedure:

1. Place slides on the rack
2. Dewax and hydrate
3. Immerse section slides in 1% Alcian blue in 3% aqueous acetic acid solution (pH 2.5) for 20 minutes
4. Rinse slides in running tap water for 5 minutes
5. Immerse slides in 0.04% fast green solution for 20 minutes
6. Rinse in running tap water for 5 minutes
7. Immerse slides in 0.1% picrosirius red solution for 30 minutes
8. Rinse in two (2) changes of acidified water for 5 minutes
9. Dehydrate in two (2) changes of 100% alcohol
10. Dip in xylene, and coverslip with Entellan mounting medium

Results

Sirius Red stained collagen, Fast Green stained non-collagenous background proteins and Alcian Blue stained the primary components of the matrix ground material, glycosaminoglycans and proteoglycans.

Appendix 9: Periodic Acid- Schiff (PAS)

Reagent Reagents used;

- 0.5% Periodic Acid Solution;

  Add 5g of Periodic Acid in 100ml of distilled water
- Schiff Reagent

  Test for Schiff reagent: A good Schiff reagent will turn a red-purple colour

Staining procedure;

11. Place slides on the rack
12. Dewax and hydrate
13. Oxidise in 0.5 % periodic acid solution for 5 minutes
14. Rinse slides in running water
15. Place in Schiff reagent for 15 minutes
16. Counterstain in Mayer's haematoxylin for 1 minute
17. Wash slides in tap water for 5 minutes
18. Dehydrate through an ascending series of alcohol changes; 70%, 95% and 100% (10 dips or 30s)
19. Dip in two changes of xylene for 2 minutes each
20. Mount slides with Entellan and coverslip

Results: The PAS stains the glycogen/mucus substances red-purplish and stained nuclei blue.

Appendix 10: Immunofluorescence Triple Labelling

Reagents Required:

For 26 slides (in paraffin) with ~ 2 sections per slide

Citrate Buffer pH6

Tri-Sodium Citrate (Di-hydrate)	2.9g
Distilled water	1000ml

Mix to dissolve and adjust pH to 6 with 1M HCl

1M Phosphate Buffer Saline pH7.4 (PBS)

- NaCl 40g
- Na_2HPO_4 8.75g
- KCl 1g
- KH_2PO_4 1g
- Distilled water 5000ml
- **Antibody Diluent (0,2% Triton in PBS)**
- PBS (1M, pH7.4) 1200ml
- Triton-X 2.4ml

Normal Goat serum (make up only the amount required for the no of slides)

Normal goat serum	80ul
PBS (1M, pH7.4)	7920ul

Primary antibody dilutions (Total Volume = 8000ul)

- **Anti-smooth muscle Actin polyclonal (1:200)**

0,2% Triton in PBS	7960 ul
Anti-smooth muscle Actin polyclonal	40 ul

- **Anti–collagen II mouse monoclonal (1:500)**

0,2% Triton in PBS	7984 ul
Anti–Collagen II mouse monoclonal	16 ul

Secondary antibody dilutions (Total Volume = 8000ul)

- **Goat Anti-Rabbit Alexa Fluor 488 (1:1000)**

PBS (1M, pH7.4)	7992 ul
Goat Anti-Rabbit Alexa Fluor 488	8 ul

- **Goat Anti-Mouse Alexa Fluor 594 (1:1000)**

PBS (1M, pH7.4)	7992 ul
Goat Anti-Mouse Alexa Fluor 594	8 ul

- **DAPI (1:10000)**

PBS (1M, pH7.4)	7999.2 ul
DAPI	0.8 ul

Fluorescent Labelling: Method

Day 1 - Antigen Retrieval

1. Dewax and hydrate slides
2. Draw circles around each section with a PAP pen
3. Place slides in Citrate Buffer pH6, overnight in a water bath @ 60° C

Day 2- SMA Incubation

1. Allow sections to cool to room temperature 20min
2. Wash in PBS/0,2% Triton –X 3 x5min
3. Block sections with 10% Normal goat serum 1hr@RT
4. Incubate with **Primary antibody (SMA)** @4°C in a humid chamber Overnight

Primary antibody dilutions:

Anti-smooth muscle Actin polyclonal (1:200)

Day 3- Alexa Flour 488 and AC2 Incubation

1. Wash in PBS 3 x10min

From this step onwards –work in the dark (FOR ALL)

2. Incubate **in the DARK** in secondary antibody
    - Goat Anti-Rabbit Alexa Fluor 488 (1:1000) 1-2 hrs @RT
3. Wash in PBS 3 x10min
4. Incubate with **Primary antibody (AC2)** @4°C in a humid chamber Overnight

Primary antibody dilutions:

Anti–collagen II mouse monoclonal (1:500)

Day 4- Alexa Flour 594 and DAPI Incubation

1. Wash in PBS 3 x10min
2. Incubate **in the DARK** in secondary antibody

- Goat Anti-Mouse Alexa Fluor 594 (1:1000) 1-2 hrs @RT

3. Wash in PBS 3 x10min
4. Incubate with DAPI in PBS (1: 8000) 5min
5. Wash in PBS 3 x 5min
6. Mount with anti-fade and store in the dark at 4°C until viewing